People's Democratic Republic of Algeria
Ministry of Higher Education and Scientific Research

University M'Hamed BOUGARA – Boumerdes

Institute of Electrical and Electronic Engineering

Department of Power and Control

Final Year Project Report Presented in Partial Fulfilment of the Requirements for the Degree of the

MASTER

Option: **Control Engineering**

Power Engineering

Title:

Modeling and Nonlinear Control of 2-DOF Helicopter "Quanser Aero2"

Presented by:

- **BAHLOUL Affaf**
- **BENAOUDA Imen**

Supervisor:

Dr. FELLAG Ratiba

Co-Supervisor:

Dr. AMMAR Abdelkarim

Registration Number:……/2023

Dedication

Praise to God, the supreme for leading us in our study path,
and for allowing us to realize this work.

First and foremost, I would like to dedicate this work to myself, above all, for being strong and dedicated and not giving up in the hardest times.

To my beloved parents, my father and dear mother, who dedicated their lives to raise me , your presence in my life is vital, without your encouragement and support;
I would not be where I am now.
Your constant care, wise advice and pure love is the secret behind my success .
Only Allah know how much I love you, and how deep is my desire to make you feel happy and proud.

To my younger siblings who brought joy to my life.

Finally, I cannot forget to mention my dear friends, the ones who had always been around me and supported me.

Bahloul Afaf

Dedication

I dedicate this work to my beloved family whose support and encouragement have been the reason behind my academic journey.

To my sisters and brother, thank you for always cheering me on. Your love and have made this journey more meaningful.

I also dedicate this work to my dear friends, who have stood by my side .

May this dedication serve as a token of gratitude for all the love, support, and belief you have shown me.

Benaouda Imen

Aknowledgment

This thesis presents the work we have done within the robotics division of the Center for Advanced Technology Development Baba Hassen - Alger.

At the end of this work, We would like to express our sincere gratitude to our supervisor Dr. Ratiba Fellag, for her invaluable guidance, expertise, and support throughout the journey.

Her feedback and encouragement have been important in shaping the quality of this work. We are truly grateful for her mentorship and for pushing us to reach our full potential.

I would like to express my deepest appreciation and gratitude to my co-supervisor, Mr. Ammar Abed Elkrim, for his invaluable contribution and support throughout our journey. Without his constant availability, patience, and encouragement we wouldn't reach what we reached today

I would like to express my gratitude to the members of the jury members for examining and evaluating this work.

Abstract

This work presents the methods for the modeling and control of a 2-degree-of-freedom (2-DOF) helicopter, specifically the Quanser Aero 2 system, using four different controllers of two types of namely classical control techniques, the Proportional-Derivative (PD), and the Linear Quadratic Regulator (LQR) controllers, as well as two nonlinear control techniques namely the sliding mode controller (SMC) and the Super-twisting controller (STC). The four controllers are mainly implemented in order to overcome the problems of control of 2-DOF helicopter systems essentially linked to the nonlinearity of the dynamic models. The nonlinear dynamic model of the system is first obtained using Lagrange formalism which is linearized after that for classical control design. The proposed control schemes are then simulated using MATLAB/Simulink and implemented in real-time on the Quanser Aero2 platform. A comparative study follows to evaluate the performance of the designed controllers for both simulation and implementation results.

Keywords: Higher order sliding mode control , Linear Quadratic Regulator, Proportional Derivative control, Quanser Aero 2, Sliding mode control,2-DOF helicopter.

Contents

List of Figures

List of Tables

List of Abbreviations

DOF	Degree Of Freedom
$VTOL$	Vertical Take-Off and Landing
UAV	Unmanned Aerial Vehicle
IMU	Inertial Measurement Unit
LQR	Linear Quadratic Regulator
PID	Proportional Integral Derivative
PD	Proportional Derivative
SMC	Sliding Mode Control
$HOSMC$	Higher Order Sliding Mode Control
STC	Super Twisting Control

List of Symbols

λ	Positive constant
τ_p	Torque acting on the pitch motor
τ_y	Torque acting on the yaw motor
V_p	Pitch motor voltage
V_y	Yaw motor voltage
F_p	Force exerted by the pitch motor
F_y	Force exerted by the yaw motor
F_g	Gravitational force
l_{cm}	Distance from the Z-axis to the center of mass
m	Total mass of the helicopter
J_p	Moments of inertia for pitch
J_y	Moments of inertia for yaw
x_d	Desired states
x	State vector
u	Input vector
y	Output vector
k_p	Proportional gain
k_d	Derivative gain
r	Reference signal
w_n	Natural frequency
PO	Percentage overshoot
t_p	Peak time
τ	Damping ratio
θ_d	Desired pitch angle
K_{pp}	Torque thrust gain from the pitch rotor
K_{py}	Cross-torque thrust gain on the pitch from the yaw rotor

K_{yy}	Torque thrust gain from the yaw rotor
K_{yp}	Cross-torque thrust gain on the yaw from the pitch rotor
P_{total}	Total potential energy of the system
T_{total}	Total kinetic energy of the system
T_{trans}	Transnational kinetic energy
$T_{rot,p}$	Rotational kinetic energy for the pitch
$T_{rot,y}$	Rotational kinetic energy for the yaw
Q_1	Generalized force for the pitch
Q_2	Generalized force for the yaw
L	Lagrangian variable
D_p	Rotary viscous friction acting on the pitch
D_y	Rotary viscous friction acting on the yaw
D_t	Thrust displacement
K_{sp}	Stiffness about the pitch axis
S	Sliding surface
e	System error
n	Relative order of the system
V	Lyapunov function
u_{eq}	Equivalent control
u_{sw}	Switching control
u_n	Discontinuous control
c_1	Pitch sliding surface parameter
c_2	Yaw sliding surface parameter
ψ_d	Desired yaw angle
k_{pp}	Proportional gain for the pitch controller
k_{dp}	Derivative gain for the pitch controller
k_{py}	Proportional gain for the yaw controller
k_{dy}	Derivative gain for the yaw controller
Q	Weighting matrix for the state variables
R	Weighting matrix for the control input
P	Riccati solution matrix
K	Gains matrix

General introduction

In recent years, helicopters have emerged as versatile aerial vehicles that play crucial roles in various industries, including transportation, emergency services, and surveillance. The precise control of their motion is of paramount importance for ensuring safe and efficient operations. There has been growing interest in the development of more advanced and effective control systems for aerial vehicles, including drones and helicopters.

The study of two-degree-of-freedom (2-DOF) helicopters develops control techniques that can stabilize the aircraft in a desired way. This research dates back to the mid-20th . Helicopters pose challenges in control engineering due to their nonlinear, unstable, and highly-coupled dynamics. Additionally, these aircraft are constantly exposed to natural environmental conditions, including inclement weather such as high winds and rainfall. Such environmental factors can severely impact the performance of helicopters and introduce external disturbances .Which necessitate accurate modeling and precise control techniques to ensure stability and effective control.

The main objective of this work is to address those control problems, specifically focusing on the Quanser Aero 2 system. Our work aims to develop effective control strategies that can accurately track the desired trajectories.

in order to analyze and compare them . This will be achieved by modeling the Quanser Aero2 system using MATLAB/SIMULINK, and to perform time domain simulations and implementations in order to analyze and compare the performance of each controller.

The work conducted during this final year project is summarized in this report, and is organized in three chapters each with precise objective. In the first chapter, we introduce helicopter systems, including their historical background and fundamental working principles. Then, we introduce the Quanser Aero2 system and its specific components. After that, we present both the nonlinear and linear models that will be later used for controllers design.

The second chapter starts with a comprehensive literature review, focusing on control techniques used for 2-DOF helicopters. We then introduce the design procedures of the proposed controllers that are : the Proportional Derivative (PD), the Linear Quadratic

Regulator (LQR), the Sliding Mode Control (SMC), and the Super Twisting controllers, specifically applied to the Quanser Aero2 system. Numerical simulations are carried out for the four different control approaches and the obtained results are analyzed and compared.

Chapter three presents the real time implementation of the developed controllers on the Quanser Aero2 system , that was held in the robotics department of the Center of Development of Advanced technologies (CDTA) ,The implemented controllers were tuned and tested on two different function the square wave function and the sinusoidal function to test the tracking of the controllers this was achieved using the MATLAB/SIMULINK as well as the QUARC software , the achieved results are analysed to evaluate and compare the effectiveness of each controller.

Finally, we conclude this work with a general conclusion and provide some perspectives for future works.

Chapter I

Description and modeling of the Quanser Aero2

I.1 Introduction

This chapter provides an overview of helicopter systems, with a specific focus on the Quanser Aero 2 system. It covers the general introduction to helicopters and introduces the Quanser Aero 2 system and its configurations. Then it presents the Quanser Aero 2 helicopter's nonlinear model for a more accurate representation of system dynamics. Additionally, a simplified linear model is introduced to facilitate control design.

I.2 Generalities about helicopters

Helicopters are a distinct type of aircraft that have the capacity to hover, take off, and land vertically, and fly in various directions, including forwards, backward, and sideways. They are utilized in a diverse range of applications, such as military operations, transportation, search and rescue, and aerial firefighting I.1 illustrates different military and civilian helicopter types. The concept of a rotary-wing aircraft dates back to ancient times, with Leonardo da Vinci's sketches in the 15th century being one of the earliest references. However, it was not until the early 20th century that significant progress was made in developing practical helicopters [1].

I.2.1 History of helicopters

Helicopters have a rich history dating back to the early 1900s, with the first successful helicopter flight achieved by Igor Sikorsky in 1939. Since then, advancements in technology have led to the development of more efficient and versatile helicopters, including those with twin rotors, coaxial rotors, and tilt rotors. We can highlight the following noteworthy events according to [1]:

Figure I.1: example of different helicopter types [2]

1. Paul Cornu's first helicopter flight (1907): French engineer Paul Cornu made the first untethered flight of a helicopter in November 1907, using a twin-rotor design [1].

2. István Petróczy and Theodore von Kármán's Tethered Helicopter (1916): Hungarian engineer István Petróczy and Hungarian-American aerospace engineer Theodore von Kármán collaborated on the development of a tethered helicopter in 1916. Their experiments with a rotor system mounted on a metal frame advanced the understanding of helicopter technology, although it did not achieve free flight[1].

3. JJuan de la Cierva's invention of the autogyro (1923): In 1923, Spanish engineer Juan de la Cierva invented the autogyro, which served as a precursor to the modern helicopter. The autogyro used an unpowered rotor to generate lift and a conventional propeller for forward thrust [1].

4. Igor Sikorsky's successful helicopter flight (1939) : Russian-born engineer Igor Sikorsky made the first successful flight of a single-rotor helicopter in 1939, using his VS-300 prototype[1].

5. Aérospatiale's introduction of the Gazelle helicopter (1967): The French aerospace company Aérospatiale introduced the Gazelle helicopter, which became widely recognized for its versatility and performance. The Gazelle was employed for various purposes, including military, civilian, and medical applications, further advancing the capabilities of helicopters[1].

6. Sikorsky X2 Technology Demonstrator (2008): Sikorsky Aircraft Corporation developed the X2 Technology Demonstrator, a prototype helicopter that incorporated advanced technologies such as coaxial rotors and a pusher propeller. The X2 demonstrated significant improvements in speed and maneuverability compared to traditional helicopters, setting new records for rotorcraft flight[3].

7. Ingenuity Mars Helicopter (2021): NASA's Ingenuity Mars Helicopter became the first aircraft to achieve powered flight on another planet. It successfully completed multiple flights in the thin Martian atmosphere, demonstrating the feasibility of rotorcraft operations in extraterrestrial environments and opening up new possibilities for aerial exploration in space [4].

The development of more efficient and versatile helicopters has been influenced by these notable works and milestones presented in I.2. In the present work, the Quanser Aero2 2-DOF helicopter prototype is used for control design, numerical simulation, and real-time implementation of linear and nonlinear control approaches.

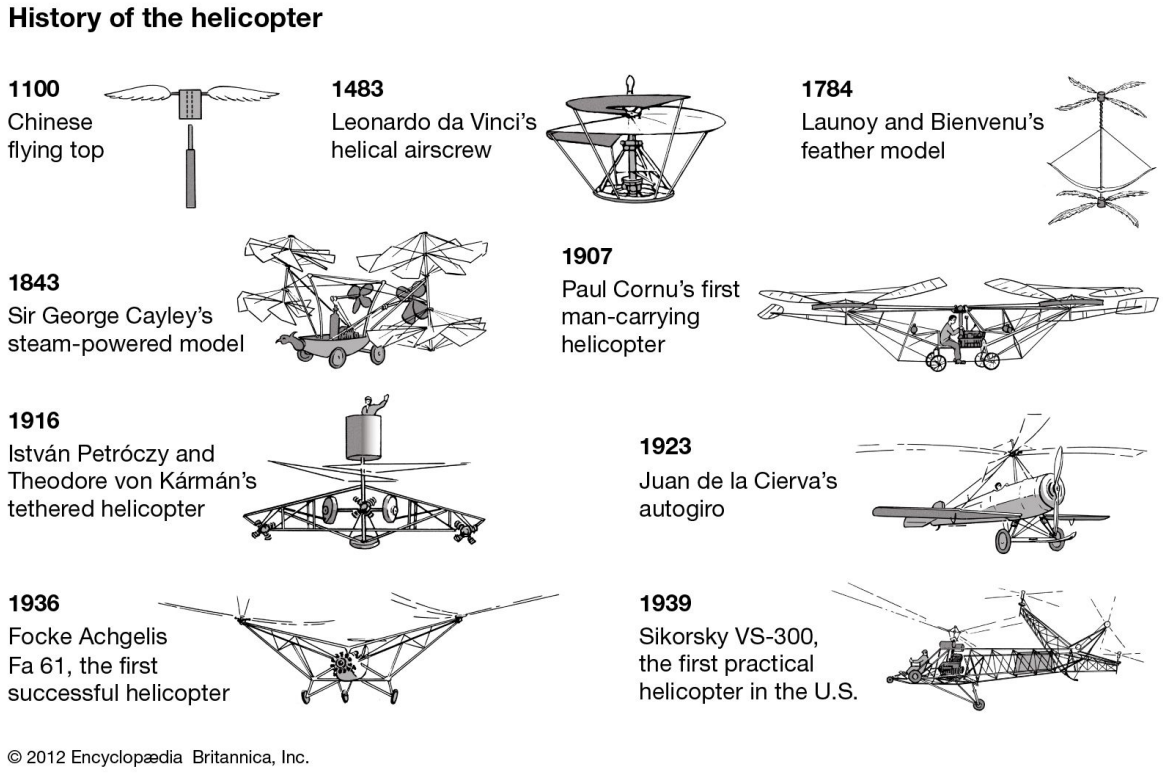

Figure I.2: Milestones in the history of the helicopter[1].

I.2.2 Operating principles of helicopters

Helicopters operate based on fundamental principles of aerodynamics. They rely on the rotation of rotor blades to generate lift. Driven by an engine, these blades create lift as they rotate through the air. The main rotor, consisting of multiple blades attached to a central hub, plays a crucial role in generating lift. As the rotor blades rotate,

they create the necessary upward force to support the weight of the helicopter and any additional payload [5].

To counteract the torque generated by the main rotor, helicopters incorporate a tail rotor as illustrated in Figure I.3. Newton's third law of motion causes the helicopter's fuselage to attempt to rotate in the opposite direction of the main rotor's rotation. The tail rotor, typically positioned at the rear of the helicopter, produces sideways thrust, effectively counteracting the torque and enabling the pilot to maintain control over the helicopter's heading.

Aside from counteracting torque, the tail rotor also plays a vital role in providing directional control. The ability to adjust the pitch of the tail rotor blades enables precise steering and maneuverability during flight, contributing to the overall control and stability of the helicopter [5].

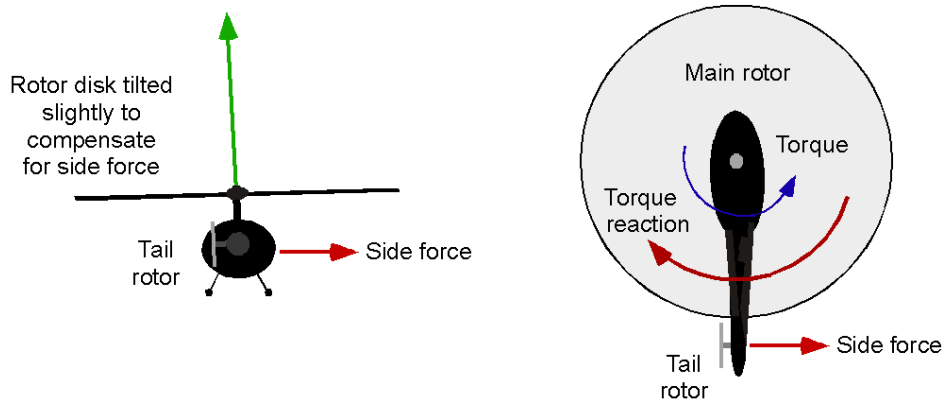

Figure I.3: Anti-Torque System for Balancing Main Rotor Torque Reaction on the Airframe [6]

I.3 The Quanser Aero2 system

The Quanser Aero2 is a widely used research platform for investigating helicopter systems, frequently employed in academic and research settings to examine different aspects of helicopter dynamics and control [7]. The Aero2 system is built to be extremely flexible, featuring a modular architecture that makes customization and expansion straightforward. Quanser Inc., a prominent supplier of sophisticated control systems and solutions, developed the Aero2 system in 2021 [7].Figure I.4 shows the different parts of the Quanser Aero 2 platform. Some of these components and their characteristics are described in the sequel [8].

I.3.1 Configurations of the Quanser Aero2 system

The Quanser Aero2 system consists of a compact helicopter model which can have three different configurations as illustrated in Figure I.5.

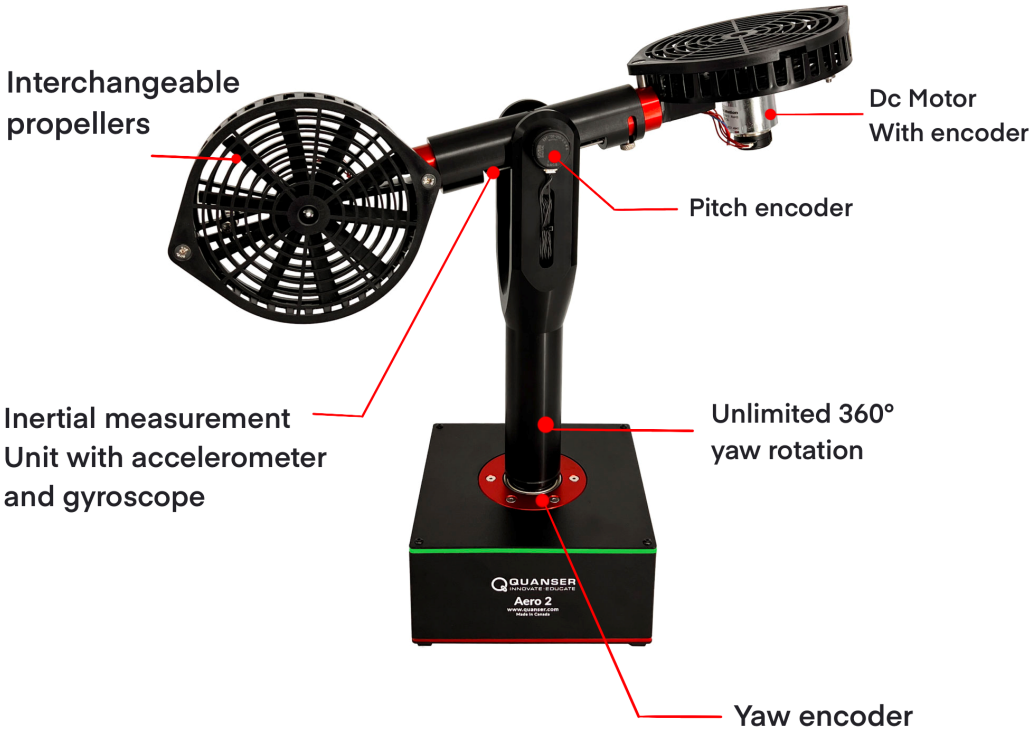

Figure I.4: The Quanser Aero 2 platform [8]

I.3.1.1 One-DOF vertical take-off and landing (VTOL)

The 1-DOF Vertical Take-Off and Landing (VTOL) configuration of the Quanser Aero2 involves controlling only one pivot while keeping the other fixed. This allows the system to move in only one degree of freedom, typically vertically, by adjusting the angles of the pitch axis, while locking the yaw axis (Figure I.5.(a)). With both rotors horizontal, this configuration is useful for developing and testing control algorithms for drones and Unmanned Aerial Vehicles (UAVs), as well as hovering in mid-air [7].

I.3.1.2 Half Quad-rotor

The Half Quad-rotor configuration (Figure I.5.(a)) of the Quanser Aero2 is designed with one pitch angle locked and one yaw angle unlocked pivot, allowing for rotation in the yaw angle but not in the pitch angle. One rotor is mounted on the unlocked pivot while the other is locked, limiting the controllability of the system. This configuration is more challenging to control and stabilize, making it an interesting option for experimentation and testing [7].

I.3.1.3 Two-DOF helicopter

As stated in [7]. The 2-DOF helicopter configuration of the Quanser Aero2 allows for simultaneous control of both pitch and yaw angles, mimicking the behavior of a helicopter with independent control of its two rotors. This configuration, illustrated in Figure I.5.(b), serves as a valuable research tool for exploring the dynamics and control

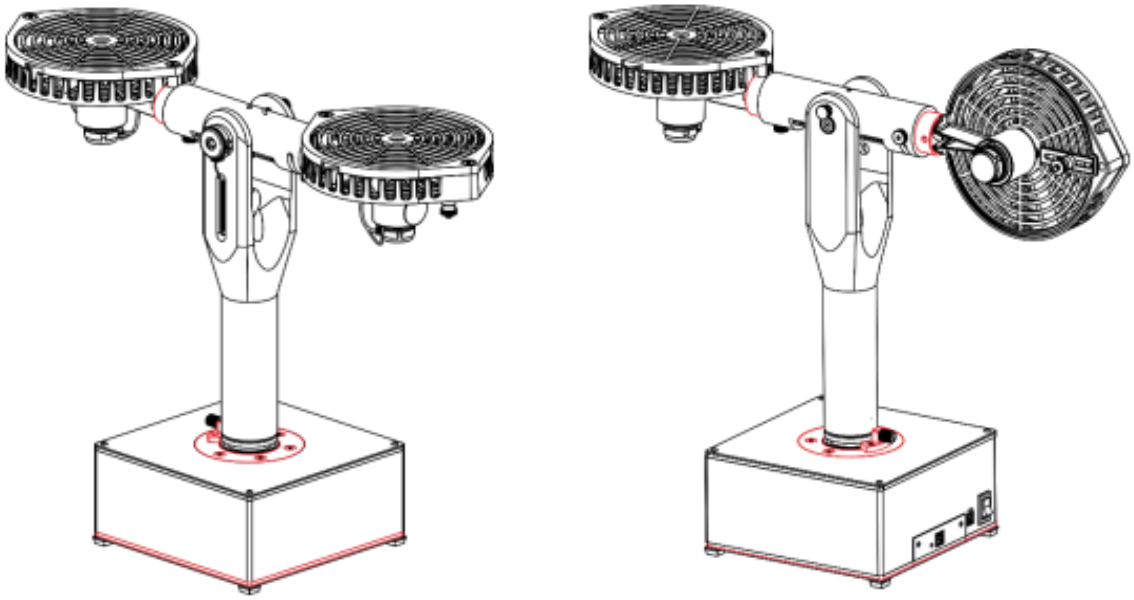

(a) Half-Quad and VTOL configuration [8] (b) 2 DOF configuration [8]

Figure I.5: Configurations of the Aero 2 system

of helicopter-like systems and advancing the field of mechatronics and flight control. Unlike the VTOL and Half quad-rotor configurations, both pitch and yaw axes are unlocked, with the head rotor horizontal and the tail rotor vertical to closely simulate a real helicopter .

I.3.2 Components of the Quanser Aero2

In this work, the main configuration we are interested in is the 2-DOF helicopter configuration where the head rotor allows elevation and the tail rotor provides a counteracting force to the helicopter's main rotor which ensures stability. The Quanser Aero2 prototype is fixed to the ground through some mechanism that allows pitch and yaw motion only. Figure I.6 shows detailed components of the Quanser Aero2 platform with their associated IDs and Table I.1 lists the different component IDs and their associated names.Some of these components and their characteristics are described in the sequel [8].

I.3.3 DC motors

The Quanser Aero 2 includes a pair of direct-drive 24V brushed DC motors. The yaw motor is responsible for actuating the back propeller, while the pitch motor rotates the front propeller. These motors are two Allied Motion CL40 Series Coreless DC Motors, model 16705, whose characteristics are detailed in the motor specifications provided in the appendix A.1 [8].

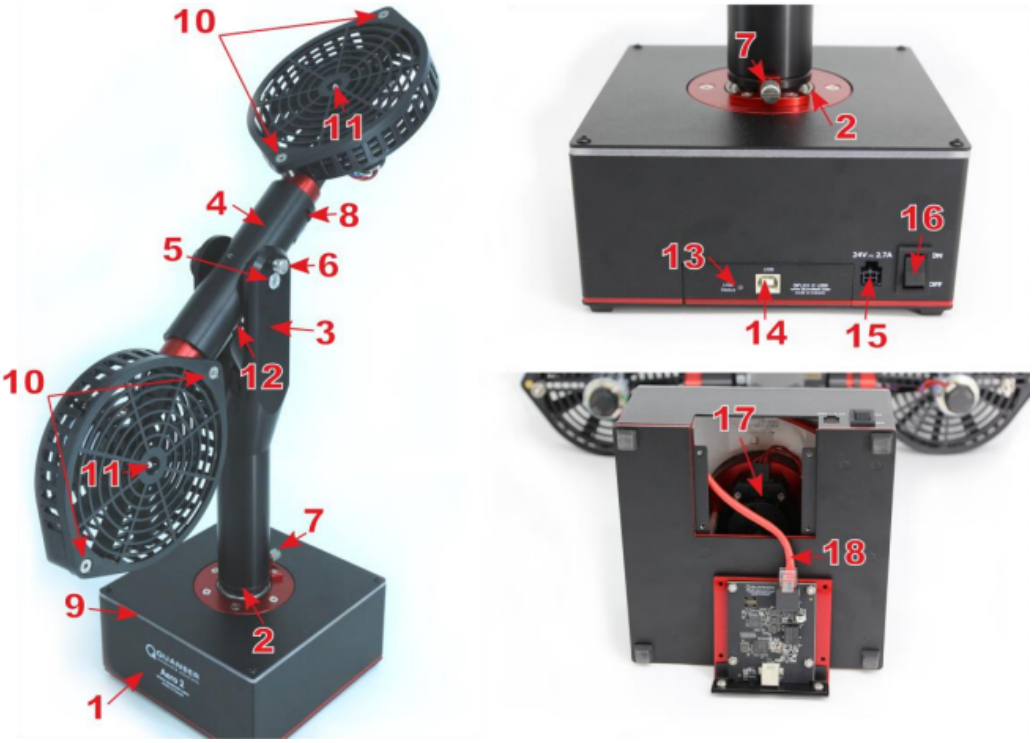

Figure I.6: Components of the Quanser Aero2 system [8]

ID	Component	ID	Component
1	Base	10	Propeller guard screws
2	Yaw pivot	11	Propeller hub
3	Support yolk	12	IMU (on Aero 2 core board)
4	Aero 2 body	13	Interface power LED
5	Pitch pivot	14	Data connector (USB version shown)
6	Pitch lock	15	Power connector
7	Yaw lock	16	Power switch
8	Thruster rotation locks	17	Yaw encoder and slip ring
9	Base LEDs	18	Aero 2 QFLEX 2 internal data bus

Table I.1: Component IDs and Components[8]

I.3.4 Propellers

The Quanser Aero 2 is equipped with two eight-vane counter-rotating 3D-printed propellers. These propellers have been specially designed to have high dynamic coupling. As such they will apply a strong cross-torque during thrust. These propellers are manufactured custom for Quanser [8].

I.3.5 Inertial Measurement Unit (IMU)

The IMU is a specific type of sensor that measures angular rate, force, and sometimes magnetic field. The Quanser Aero2 has a 6-axis IMU mounted on the Aero core board, consisting of a 3-axis gyroscope that has a 16-bit, +/-500 deg/s range and an accelerometer that has a 16-bit, +/-8g range. The gyroscope measures angular velocity

while the accelerometer measures acceleration. Combining data from both sensors using sensor fusion techniques allows for accurate determination of the body's position and orientation. The IMU incorporated into the Quanser Aero 2 is the TDK IIM-42652 inertial module [8].

I.3.6 Encoders

As depicted in Figure I.4, there are three different types of encoders on the Quanser Aero 2. The encoders used to measure the pitch of the Aero body and the angular position of the DC motors on the Quanser Aero 2 are single-ended optical shaft encoders. The motor encoders output 2048 counts per revolution in quadrature mode (512 lines/rev). This encoder is the US Digital E8P-512-118 single-ended optical shaft encoder. While the pitch encoder is 2880 counts per revolution in quadrature mode (720 lines/rev) consisting of a US Digital E8P-720-118 single-ended optical shaft encoder.

The final encoder used to measure the yaw position of the support yolk is the US Digital E3-1024-984 optical encoder, which outputs 4096 counts per revolution in quadrature (1024 lines/rev) [8].

I.4 Modeling of the Quanser Aero2 2-DOF helicopter

I.4.1 Derivation of the nonlinear model

In control engineering, modeling is an indispensable step in the process of designing effective control systems for physical systems. Modeling involves creating a mathematical model of the system that accurately captures its dynamics and behavior. By obtaining an accurate representation of the system, the control design can be more effective. Figure I.7 depicts the free-body diagram of the Aero2 model, which includes both vertical and horizontal forces. Applying a voltage V_p to the pitch motor of the Quanser Aero2 helicopter generates a perpendicular force, F_p, that acts on the body at a distance r_p from the Z-axis along the X-axis. This force causes the propeller to rotate, generating a motion about the pitch rotor motor shaft that is then transferred to the yaw axis. Due to this transfer, the rotation of the pitch propeller affects not only the pitch axis but also the yaw axis, which is why traditional helicopters use a tail rotor or anti-torque rotor to counterbalance the torque produced around the yaw axis by the main rotor [10].

Similarly, the yaw motor produces a force F_y that acts on the body at a distance r_y from the yaw axis, and thus controls the yaw motion via the back or tail propeller. Additionally, the body experiences a gravitational force F_g at a distance of l_{cm} from the Z-axis. As you can see clearly in figure I.7 the gravitational force is applied at the center of mass which is at a distance l_{cm} from the z-axis To accurately model the system

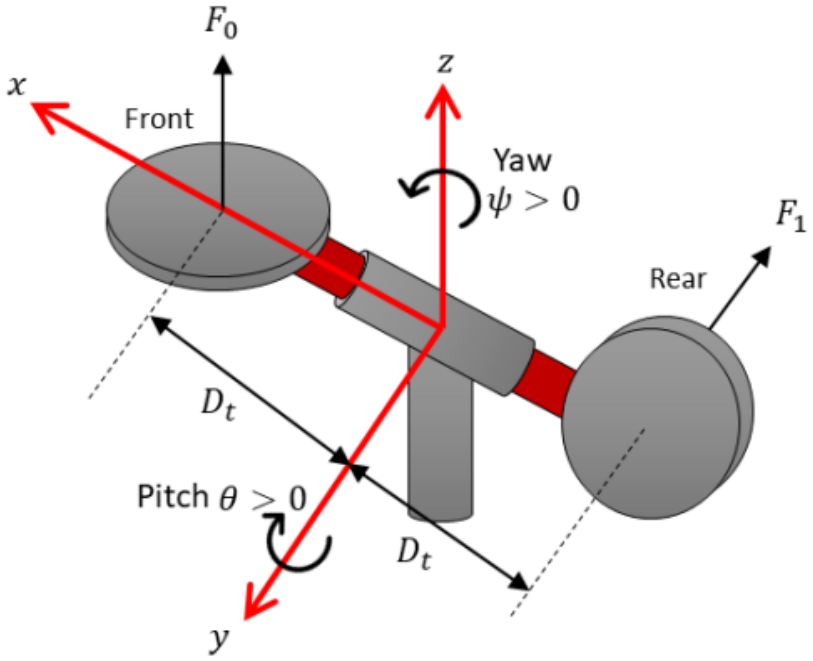

Figure I.7: Simple free-body diagram of Quanser Aero2 system [9]

dynamics, it is crucial to determine the position of the center of mass with respect to the fixed frame (pivot) of the Quanser Aero2 system, this is one using homogeneous transformation matrices [11], the derived Cartesian coordinates are :

$$X_{cm} = l_{cm}\cos(\theta)\cos(\psi), \quad Y_{cm} = -l_{cm}\cos(\theta)\sin(\psi), \quad Z_{cm} = l_{cm}\cos(\theta) \tag{I.1}$$

The complete potential energy of the system is contributed by the gravitational force alone.

$$P_{total} = mgl_{cm}\cos(\theta) \tag{I.2}$$

where m defines the total mass of the helicopter. The overall kinetic energy of the system is the summation of rotational kinetic energy and transnational kinetic energy[10].

$$T_{total} = T_{rot,p} + T_{rot,y} + T_{trans} \tag{I.3}$$

$$T_{rot,p} = \frac{1}{2}J_p\dot{\theta}^2, \qquad T_{rot,y} = \frac{1}{2}J_y\dot{\psi}^2 \tag{I.4}$$

The moments of inertia for pitch and yaw are denoted by J_p and J_y, respectively. The expression for the transnational kinetic energy is [10]:

$$T_{trans} = \frac{1}{2}m\left(X_{cm}^2 + Y_{cm}^2 + Z_{cm}^2\right) \tag{I.5}$$

substituting the expressions (I.4) and (I.5) into (I.3), the total kinetic energy is obtained as:

$$T_{total} = \frac{1}{2}J_p\dot{\theta}^2 + \frac{1}{2}J_y\dot{\psi}^2 + \frac{1}{2}ml_{cm}^2\left(\cos^2\theta\dot{\psi}^2 + \dot{\theta}^2\right) \tag{I.6}$$

The Lagrangian variable L is now defined to represent the difference between the kinetic and potential energy of the system, providing a useful tool for analyzing the dynamics of the system[12].

$$L = T_{total} - P_{total} \tag{I.7}$$

Substituting (I.3) and (I.2) into the latter defined equation (I.7) , we obtain the equation of the Lagrangian variable as follows :

$$L = \frac{1}{2}J_p\dot{\theta}^2 + \frac{1}{2}J_y\dot{\psi}^2 + \frac{1}{2}ml_{cm}^2(\cos^2\theta\dot{\psi}^2 + \dot{\theta}^2) - mgl_{cm}\sin\theta \tag{I.8}$$

The set of differential equations used to derive the equations of motion in Euler-Lagrange method are as follows:

$$\frac{\partial L}{\partial \theta} - \frac{\partial}{\partial t}\frac{\partial L}{\partial \dot{\theta}} = -Q_1 \qquad \frac{\partial L}{\partial \psi} - \frac{\partial}{\partial t}\frac{\partial L}{\partial \dot{\psi}} = -Q_2 \tag{I.9}$$

One can also derive the generalized forces Q1 and Q2 as follows:

$$Q_1 = D_tK_{pp}V_p + D_tK_{py}V_y - D_p\dot{\theta} \qquad Q_2 = D_tK_{yp}V_p + D_tK_{yy}V_y - D_y\dot{\psi} \tag{I.10}$$

where D_p is the damping about the pitch axis,K_{pp} is torque thrust gain from the pitch rotor and K_{py} is the cross-torque thrust gain acting on the pitch from the yaw rotor, accordingly D_y is the damping about the yaw axis,K_{yy} is torque thrust gain from the yaw rotor and K_{yp} is the cross-torque thrust gain acting on the yaw from the pitch rotor. Hence we determine :

$$\frac{\partial L}{\partial \theta} = -mgl_{cm}\cos(\theta) - ml_{cm}^2\sin(\theta)\cos(\theta)\dot{\psi}^2 \tag{I.11}$$

$$\frac{\partial}{\partial t}\left(\frac{\partial L}{\partial \dot{\theta}}\right) = J_p\ddot{\theta} + ml_{cm}^2\ddot{\theta} \tag{I.12}$$

From the above equations, we get

$$J_p\ddot{\theta} + ml_{cm}^2\ddot{\theta} + mgl_{cm}\cos(\theta) + ml_{cm}^2\sin(\theta)\cos(\theta)\dot{\psi}^2 = D_tK_{pp}V_p + D_tK_{py}V_y - D_p\dot{\theta} \tag{I.13}$$

$$\ddot{\theta} = \frac{1}{J_p + ml_{cm}^2}\left[D_tK_{pp}V_p + D_tK_{py}V_y - D_p\dot{\theta} + mgl_{cm}\cos(\theta) + ml_{cm}^2\sin(\theta)\cos(\theta)\dot{\psi}^2\right] \tag{I.14}$$

Similarly, we get for the yaw axis angle ψ.

$$\ddot{\psi} = \frac{1}{J_y + ml_{cm}^2\cos^2(\theta)}\left[D_tK_{yp}V_p + D_tK_{yy}V_y - D_y\dot{\psi} + 2ml_{cm}^2\sin(\theta)\cos(\theta)\dot{\psi}\dot{\theta}\right] \tag{I.15}$$

The equations of motion are defined by the following variables K_{pp}, K_{py},K_{yp}, and K_{yy}, which will be later estimated. V_p and V_y denote the voltages applied to the pitch and yaw motors, and D_t is the thrust displacement. The torque applied on the pitch

and yaw axes is cross-coupled, as seen in equation (I.10). The notations below are defined to simplify the model:(I.14) and (I.15) become :

$$\ddot{\theta} = \frac{1}{a}\left[D_t K_{pp} V_p + D_t K_{py} V_y - D_p \dot{\theta} + mgl_{cm}\cos(\theta) + ml_{cm}^2 \sin(\theta)\cos(\theta)\dot{\psi}^2\right] \tag{I.16}$$

and

$$\ddot{\psi} = \frac{1}{b}\left[D_t K_{yp} V_p + D_t K_{yy} V_y - D_y \dot{\psi} + 2ml_{cm}^2 \sin(\theta)\cos(\theta)\dot{\psi}\dot{\theta}\right] \tag{I.17}$$

Where $a = J_p + ml_{cm}^2$ and $b = J_y + ml_{cm}^2 \cos^2\theta$.

Equation (I.16) and (I.17) are the final equations of the nonlinear model that will be later used in the development of the nonlinear controllers, these equations are in terms of the parameters that were estimated as described in the appendix A.2 and their numerical values are provided in Table I.2.

Symbol	Parameter description	Value (unit)
J_p	Total moment of inertia about pitch axis	0.0232 kg m^2
J_y	Total moment of inertia about yaw axis	0.0238 kg m^2
D_p	Equivalent viscous damping about pitch axis	0.00199 N/V
D_y	Equivalent viscous damping about yaw axis	0.00192 N/V
k_{pp}	Thrust force constant of yaw motor/propeller	0.00321 N m/V
k_{yy}	Thrust torque constant of yaw axis from yaw motor/propeller	0.00610 N m/V
k_{py}	Thrust torque constant acting on pitch axis from yaw motor/propeller	0.00137 N m/V
k_{yp}	Thrust torque constant acting on yaw axis from pitch motor/propeller	-0.00319 N m/V
m	Total moving mass of the helicopter	1.07 kg
l_{cm}	Center of mass length along helicopter body from pitch axis	0.0024 m
K_{sp}	Friction or stiffness of the system	0.00884 N-m/rad
D_t	Thrust displacement	0.168 m
g	Gravitational acceleration	9.81 m/s^2
V_p	Pitch motor voltage	± 24 V
V_y	Yaw motor voltage	± 24 V

Table I.2: Quanser Aero 2 System Parameters[8]

I.4.2 Derivation of the linear model

The nonlinear model presented in section I.4.1 is complex, making controller design challenging. To simplify the system and enable easier analysis and control strategy design, a linear model is commonly derived. The linear model is obtained using simplified equations and small-angle approximation, providing a straightforward representation of the system dynamics, and its simplicity and ease of implementation make it a preferred choice in control design [9].

To obtain this linear model, we can use the following set of equations when the body is parallel to the ground :

$$J_p \ddot{\theta} + D_p \dot{\theta} + K_{sp}\theta = \tau_p \tag{I.18}$$

$$J_y \ddot{\psi} + D_y \dot{\psi} = \tau_y \tag{I.19}$$

where the torques acting on the pitch and yaw axes are :

$$\tau_p = D_t K_{pp} V_p + D_t K_{py} V_y, \quad \text{and} \quad \tau_y = D_t K_{yp} V_p + D_t K_{yy} V_y. \tag{I.20}$$

substituting (I.18) and (I.19) in (I.20) We obtain:

$$J_p \ddot{\theta} + D_p \dot{\theta} + K_{sp} \theta = D_t K_{pp} V_p + D_t K_{py} V_y \tag{I.21}$$

$$J_y \ddot{\psi} + D_y \dot{\psi} = D_t K_{yp} V_p + D_t K_{yy} V_y \tag{I.22}$$

The equations above are in terms of the parameters described in Table I.2.

I.4.2.1 Transfer function model

Taking the Laplace transform of the equations of motion along the pitch axis given in (I.21), we get :

$$J_p \left(\theta(s)s^2 - \theta(0^-)s - \dot{\theta}(0^-)\right) + D_p \left(\theta(s)s - \theta(0^-)\right) + K_{sp}\theta(s) = D_t K_{pp} V_p(s) + D_t K_{py} V_y(s) \tag{I.23}$$

and the equation of motion along the yaw axis given in (I.22) we get :

$$J_y(\psi(s)s^2 - \psi(0^-)s - \dot{\psi}(0^-)) + D_y(\psi(s)s - \psi(0^-)) = D_t K_{yp} V_p(s) + D_t K_{yy} V_y(s) \tag{I.24}$$

Because this is a multi-input multi-output (MIMO) system with two outputs and two inputs, the system is represented as a set of four transfer functions:
$\frac{\theta(s)}{V_p(s)}$ and $\frac{\theta(s)}{V_y(s)}$ for pitch, and $\frac{\psi(s)}{V_p(s)}$ and $\frac{\psi(s)}{V_y(s)}$ for yaw respectively [9].

Using this and assuming all the initial conditions are zero we obtain the following transfer functions describing the system motions relative to the different inputs:

$$\frac{\theta(s)}{Vp(s)} = \frac{D_t K_{pp}}{J_p s^2 + D_p s + K_{sp}} \qquad \frac{\psi(s)}{Vp(s)} = \frac{D_t K_{yp}}{J_y s^2 + D_y s} \tag{I.25}$$

and :

$$\frac{\theta(s)}{Vy(s)} = \frac{D_t K_{py}}{J_p s^2 + D_p s + K_{sp}} \qquad \frac{\psi(s)}{Vy(s)} = \frac{D_t K_{yy}}{J_y s^2 + D_y s} \tag{I.26}$$

I.4.2.2 Linear state-space representation

One way to express this model is by using the state space representation, which can be given as:

$$\begin{cases} \dot{x}(t) = Ax(t) + Bu(t) \\ y(t) = Cx(t) + Du(t) \end{cases} \tag{I.27}$$

Rearranging eq (I.21) and (I.22) we get :

$$\ddot{\theta} = \frac{-D_p}{J_p}\dot{\theta} - \frac{K_{sp}}{J_p}\theta + \frac{D_t K_{pp}}{J_p}V_p + \frac{D_t K_{py}}{J_p}V_y \tag{I.28}$$

$$\ddot{\psi} = -\frac{D_y}{J_y}\dot{\psi} + \frac{D_t K_{yp}}{J_y}V_p + \frac{D_t K_{yy}}{J_y}V_y \tag{I.29}$$

Introducing x(t) as the state vector which we define for the Quanser Aero2 Experiment as :

$$\boldsymbol{x}^T = \begin{bmatrix} x_1 & x_2 & x_3 & x_4 \end{bmatrix} = \begin{bmatrix} \theta(t) & \psi(t) & \dot{\theta}(t) & \dot{\psi}(t) \end{bmatrix} \tag{I.30}$$

$u(t)$ is the input vector, defined as :

$$\boldsymbol{u}^T = \begin{bmatrix} V_p & V_y \end{bmatrix}. \tag{I.31}$$

$y(t)$ is the output vector defined as :

$$\boldsymbol{y}^T = \begin{bmatrix} y_1 & y_2 \end{bmatrix}. \tag{I.32}$$

The matrices A, B, C, and D represent the system dynamics and input/output relationships, and have the following dimensions: $A : 4\times 4$, $B : 4\times 2$, $C : 2\times 4$, and $D : 2\times 2$ We can write the model in terms of the states and control input as follows:

$$\begin{cases} \dot{x}_1 = x_3 \\ \dot{x}_2 = x_4 \\ \dot{x}_3 = -\dfrac{D_p}{J_p}x_1 - \dfrac{K_s p}{J_p}x_3 + \dfrac{D_t K_{pp}}{J_p}u_1 + \dfrac{D_t K_{py}}{J_p}u_2 \\ \dot{x}_4 = -\dfrac{D_y}{J_y}x_4 + \dfrac{D_t K_{yy}}{J_y}u_1 + \dfrac{D_t K_{yp}}{J_y}u_2 \\ y_1 = x_1 \\ y_2 = x_2 \end{cases} \tag{I.33}$$

And in matrix format as follows :

$$\begin{cases} \dot{x} = \begin{bmatrix} 0 & 0 & 1 & 0 \\ 0 & 0 & 0 & 1 \\ -\frac{K_s p}{J_p} & 0 & -\frac{D_p}{J_p} & 0 \\ 0 & 0 & 0 & -\frac{D_y}{J_y} \end{bmatrix} x + \begin{bmatrix} 0 & 0 \\ 0 & 0 \\ \frac{D_t K_{pp}}{J_p} & \frac{D_t K_{py}}{J_p} \\ \frac{D_t K_{yp}}{J_y} & \frac{D_t K_{yy}}{J_y} \end{bmatrix} u \\ y = \begin{bmatrix} 1 & 0 & 0 & 0 \\ 0 & 1 & 0 & 0 \end{bmatrix} x \end{cases} \tag{I.34}$$

These state-space matrices, namely the system matrix A, input matrix B, and output matrix C, play a fundamental role in analyzing the system's behavior.

I.4.2.3 Controllability

The controllability of a system is an important step that must be considered before designing a controller, as it determines the system's ability to achieve desired states or trajectories through control inputs[13]. Without assessing the controllability of a system, any further actions taken to design a controller would be invalid. Therefore, understanding the controllability characteristics of the Quanser Aero2 system, becomes a fundamental step in developing effective control strategies.

Introducing the controllability matrix C as [13] :

$$\mathbf{C} = \begin{bmatrix} \mathbf{B} & \mathbf{AB} & \mathbf{A^2B} & \dots & \mathbf{A^{n-1}B} \end{bmatrix} \tag{I.35}$$

where:

$\mathbf{C}$ is the controllability matrix,

$\mathbf{A}$ is the state matrix of the system,

$\mathbf{B}$ is the input matrix of the system,

n is the number of state variables in the system.

the state vector given in (I.27) is a 1×4 vector meaning $n = 4$.

$$\mathbf{C} = \begin{bmatrix} \mathbf{B} & \mathbf{AB} & \mathbf{A^2B} & \mathbf{A^3B} \end{bmatrix} \tag{I.36}$$

Substituting matrix B and A from (I.34)in (I.36) .

$$C = \begin{bmatrix} 0 & 0 & 0.023 & 0.009 & -0.002 & -0.0009 & -0.009 & -0.004 \\ 0 & 0 & -0.0225 & 0.043 & 0.002 & -0.003 & -0.0001 & 0.0003 \\ 0.023 & 0.009 & -0.002 & -0.0009 & -0.009 & -0.004 & 0.001 & 0.0006 \\ -0.022 & 0.043 & 0.002 & -0.003 & -0.0001 & 0.0003 & 0 & 0 \end{bmatrix} \tag{I.37}$$

upon examining the rank of the controllability matrix we find that $rank(C) = 4$, thus the controllability matrix C is full rank which indicates the controllability of the Quanser Aero2 system .

I.5 Conclusion

In conclusion, this chapter has provided a historical and technical overview of helicopters, with a specific emphasis on the Quanser Aero 2 model. We presented the nonlinear and linear models of the Quanser Aero 2 helicopter. Moving forward, the next chapter will provide the design of control techniques specifically introduced for helicopter systems. Using various control methodologies and algorithms that can effectively handle the nonlinear and highly-coupled dynamics of helicopters to achieve trajectory tracking.

Chapter II

Controllers design

II.1 Introduction

This chapter presents a comprehensive review of control techniques for 2-DOF helicopter systems. It introduces four specific linear and nonlinear control techniques, that are : PID controller, LQR controller, sliding mode controller (SMC), and higher order sliding mode controller (HOSMC) i.e. the super twisting controller. This chapter provides detailed design steps for each approach, highlighting their performance capabilities. Practical insights are provided through simulation schematics. The obtained results demonstrate the trajectory-tracking capabilities of each technique for the Quanser Aero2 helicopter system.

II.2 Control approaches for the Quanser Aero2 helicopter: a literature review

Over the years, controller design for 2-DOF helicopter systems has gained considerable interest in the research community [14] [15] [16]. Various control approaches have been proposed to address stabilization, trajectory tracking, and robustness issues. The conventional PID controller is widely used for closed control loops due to its simplicity, it struggles to achieve satisfactory performance across the full range of disturbances without external compensation. Hence, there is a desire to develop robust control strategies that do not require additional computational effort [17].

In a study by [18], a Linear Quadratic Gaussian control was implemented for real-time tracking on a 2-DOF helicopter system. Although this approach exhibited stability and control accuracy, it struggled with the highly nonlinear and uncertain dynamics of the helicopter, leading to high-amplitude oscillations in the steady state. To overcome these challenges, researchers have explored alternative techniques.

A robust LQR for attitude control of a 2-DOF helicopter introduced by [19] employed an adaptive LQR with a Model Reference Adaptive Control (MRAC) scheme to address

tracking problems in the Quanser Aero2 helicopter. According to these advancements, there remains a need to enhance the robustness of these control strategies, particularly in the presence of aggressive turbulence effects.

Nonlinear control techniques have also shown promising results in handling the highly nonlinear dynamics of the helicopter system. SMC and backstepping control [10] are two notable nonlinear control methods. Several sliding mode control structures have been investigated in the literature for controlling a 2-DOF helicopter system [20]. These structures combine SMC and LQR techniques, where the LQR stabilizes the yaw and pitch channels while the SMC ensures robustness against external disturbances [21]. Another approach, proposed by [22], employs a super-twisting 2-sliding mode control (2-SMC) to handle uncertainty arising from variations in mass distribution. In 2022, Reyhanoglu et al. presented a study on developing a learning-based robust trajectory tracking control strategy for a 2-DOF helicopter system [23]. The authors aimed to address the challenges associated with achieving accurate trajectory tracking in the presence of uncertainties and disturbances. To tackle this, they combined a tdegreesitional PID controller with reinforcement learning techniques. The PID controller served as the foundation, providing a well-established control framework, while reinforcement learning enabled online learning and adaptation of controller parameters. By optimizing the controller through learning algorithms, the proposed approach aimed to improve trajectory tracking accuracy. The study included simulations and experiments to validate the effectiveness of the approach.

In this work, we focus on implementing two linear control approaches (PD and LQR) and two nonlinear ones (SMC, and Super twisting) to achieve trajectory tracking of the 2-DOF Quanser Aero 2 helicopter platform. A comparison will follow based on simulation and experimentation tests.

II.3 Proportional-Derivative controller (PD)

Proportional-Derivative (PD) control is a classical control technique used to regulate the behavior of dynamic systems. It is widely used in process control, aircraft control, and robotics[17]. Most systems employ either open-loop or closed-loop control methods. In open-loop control, the control effort is based solely on the output variable and does not take into account feedback from the system. In contrast, closed-loop control uses feedback from the system to adjust the control effort and maintain the output variable at the desired set point [24].

The objective of the control design is to regulate the pitch and yaw angles of the Quanser Aero2 helicopter to desired trajectories. To achieve this goal, a state-feedback controller is developed based on the system's linear model developed in the previous chapter.

II.3.1 Controller design

The PD control presented in this section and illustrated in Figure II.1 is a modified version of the conventional PD control technique, where only the negative velocity is utilized as feedback. This modification is specifically adopted to address the coupled nature of the Quanser Aero2 system and achieve effective control of the pitch and yaw angles. By focusing solely on the negative velocity feedback, the control strategy aims to mitigate the interdependency between the angles and minimize the undesired coupling effects[17]. Furthermore, a low-pass filter is incorporated in the derivative term to reduce the impact of measurement noise.

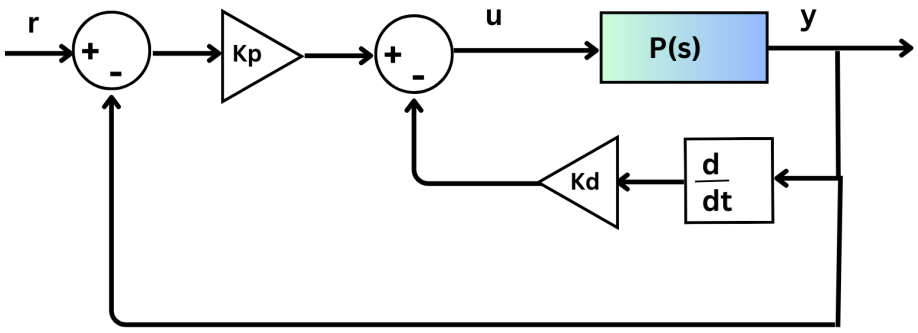

Figure II.1: Proportional-Derivative (PD) control

From Figure II.1, the PD control has the following structure:

$$u = k_p(r(t) - y(t)) - k_d\dot{y}(t) \tag{II.1}$$

The expression in the above equation relates to the PD control for the pitch axis, where k_p and k_d represent the proportional and derivative (velocity) gains, respectively. Here, $r = \theta_d(t)$ denotes the reference pitch angle, $y = \theta(t)$ stands for the measured pitch angle, and $u = V_p(t)$ corresponds to the control input or the voltage applied to the pitch rotor[9].

In the case of PD control for the yaw axis, the reference or desired yaw angle is used as the input $r = \psi_d(t)$, the measured variable corresponds to the current yaw angle $y = \psi(t)$, and the control input represents the voltage applied to the rear yaw rotor $u = V_y(t)$.

From equations (I.25) and (I.26), we obtain the decoupled transfer functions of the pitch and the yaw axis as follows:

$$P_p(s) = \frac{\theta(s)}{V_p(s)} = \frac{(D_t K_{pp}/J_p)}{s^2 + (D_p/J_p)s + (K_{sp}/J_p)} \tag{II.2}$$

and :

$$P_y(s) = \frac{\psi(s)}{V_y(s)} = \frac{(D_t K_{yy}/J_y)}{s^2 + (D_y/J_y)s} \tag{II.3}$$

As discussed in section I.4.2.2, since the Aero2 model starts from a resting state, its initial conditions are $\theta(0^-) = 0$ and $\dot{\theta}(0^-) = 0$. Applying the Laplace transform to (II.1) yields the closed-loop transfer function for the pitch-only axis as $\frac{Y(s)}{R(s)} = \frac{\theta(s)}{\theta_d(s)}$, where $\frac{Y(s)}{R(s)}$ represents the transfer function relating the output response $Y(s)$ to the input reference $R(s)$.

$$U(s) = k_p(R(s) - Y(s)) - k_d s Y(s) \tag{II.4}$$

Knowing that the control input is the voltage of the front/pitch motor, $U(s) = Vp(s)$, we can determine the closed-loop transfer function by incorporating the proportional-derivative (PD) control into the pitch transfer function. We can then solve for $\frac{Y(s)}{R(s)}$.

$$\frac{Y(s)}{R(s)} = \frac{(DtK_{pp}K_p/Jp)}{s^2 + ((Dp + DtK_{pp}K_d)/Jp)s + ((K_{sp} + DtK_{pp}K_d)/Jp)} \tag{II.5}$$

Employing the conventional transfer function prototype of second-order systems :

$$\frac{Y(s)}{R(s)} = \frac{\omega_n^2}{s^2 + 2\zeta\omega_n s + \omega_n^2} \tag{II.6}$$

These equations allow us to represent the PD control gains in terms of the desired natural frequency ω_n and damping ratio ζ, for the pitch-axis:

$$k_p = \frac{J_p\omega_n^2 - K_{sp}}{D_t K_{pp}} \tag{II.7}$$

$$k_d = \frac{2J_p\zeta\omega_n - D_p}{D_t K_{pp}} \tag{II.8}$$

By utilizing the identical control design, we can obtain the PD equations for the yaw-axis:

$$k_p = \frac{J_y\omega_n^2 - K_{sp}}{D_t K_{yy}} \tag{II.9}$$

$$k_d = \frac{2J_y\zeta\omega_n - D_y}{D_t K_{yy}} \tag{II.10}$$

To derive the values of the required natural frequency and damping ratio based on the overshoot and peak time specifications, we can use the following equations. It's important to note that in a second-order system, the damping ratio parameter is solely responsible for determining the magnitude of overshoot (PO).

$$PO = 100e^{-\frac{\pi\zeta}{\sqrt{1-\zeta^2}}} \tag{II.11}$$

Both the damping ratio ζ and natural frequency of the system ω_n contribute to the peak time t_p, which can be calculated using the following formula:

$$t_p = \frac{\pi}{\omega_n \sqrt{1-\zeta^2}} \tag{II.12}$$

In general, the damping ratio impacts the response's shape, whereas the natural frequency influences the response's speed. It's important to note that the decoupled control design, which considers each axis as a single-input, single-output (SISO) system and separately designs PD control for pitch and yaw axes, does not account for reaction torque effects mentioned in the 2 DOF helicopter modeling lab. This approach, called a decoupled controller, can lead to unexpected motions when simultaneously controlling both axes to a desired reference command. For instance, when the yaw tracks a reference command signal, it can cause a significant overshoot in the pitch axis [9].

For designing the PD gains the following set of specifications are used:

1. Peak time: tp $<$ 2.5 s for pitch angle and tp $<$ 3.5 s for yaw angle.
2. Percent Overshoot: PO $<$ 5 for both axes.

II.3.2 Simulation results

The pitch and yaw PD control of the Aero2 2-DOF helicopter are simulated using the transfer functions of the pitch and yaw respectively (II.2), (II.3) with the controller gains calculated from equations (II.8), (II.9), (II.7), and (II.9), the following schematic diagram depicted in Figure II.2.

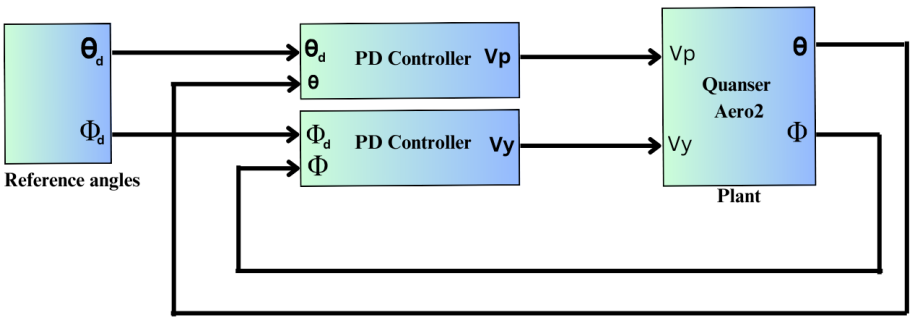

Figure II.2: PD controller simulation schematic

We set the initial conditions of the Aero2 model to 0, representing its resting state at the start of the simulation. The controller gains used in the simulation are listed in Table II.1 :

Pitch	$k_{p_p} = 116.2420$	$k_{d_p} = 99.6990$
Yaw	$k_{p_y} = 35.8626$	$k_{d_y} = 38.0289$

Table II.1: The gains for the PD controller simulation

II.3.2.1 Sinusoidal waveform tracking

This simulation incorporates a sinusoidal function as the desired input signal to test the tracking of the system, defined as:

$$\begin{cases} \theta_d = 10 \cdot \sin(2\pi \cdot 0.05 \cdot t) \\ \phi_d = 20 \cdot \sin(2\pi \cdot 0.04 \cdot t) \end{cases} \tag{II.13}$$

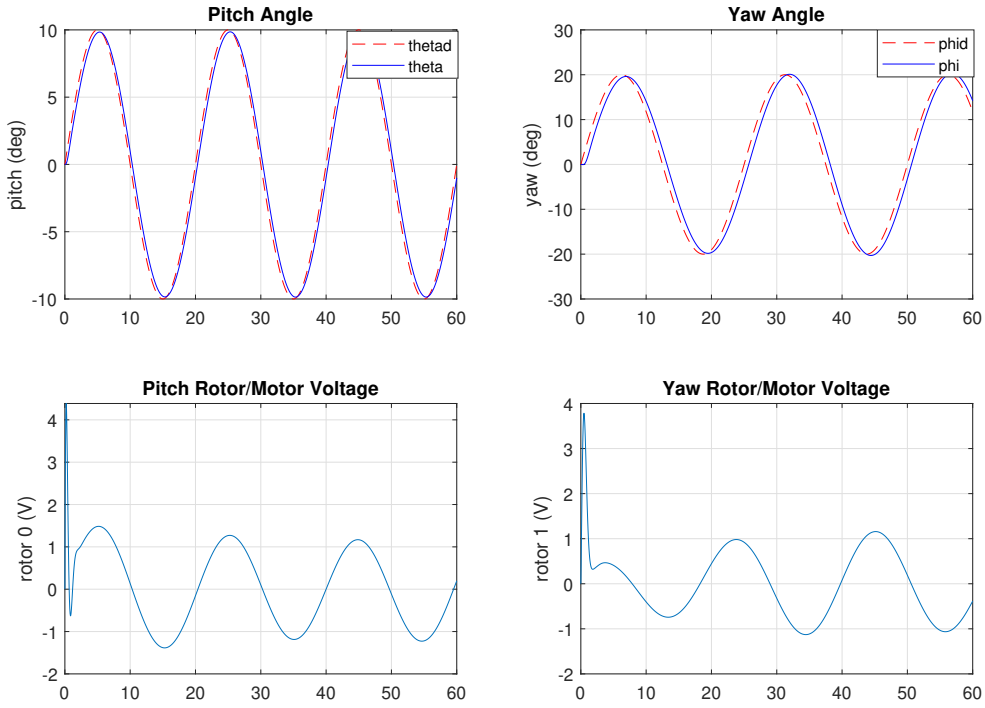

Figure II.3: Simulation results using PD controller for sinusoidal trajectory tracking

Figure II.3 presents a graphical representation of the desired angles and their corresponding actual angles obtained from the simulation.We can clearly observe the performance of the PD controller in accurately tracking the pitch and yaw angles of the system to the desired ones. The figure also includes the output voltages applied to the front/pitch motor and tail/yaw motor which shows smooth control action the motor never saturates and is always within the desired range of $\pm 24V$.

II.3.2.2 Square wave tracking

To assess the tracking capabilities of the system, this simulation utilizes a desired input signal in the form of a square function. The pitch signal has an amplitude of 10 degrees and a frequency of 0.05 Hertz, while the yaw signal has an amplitude of 20 degrees and a frequency of 0.04 Hertz.

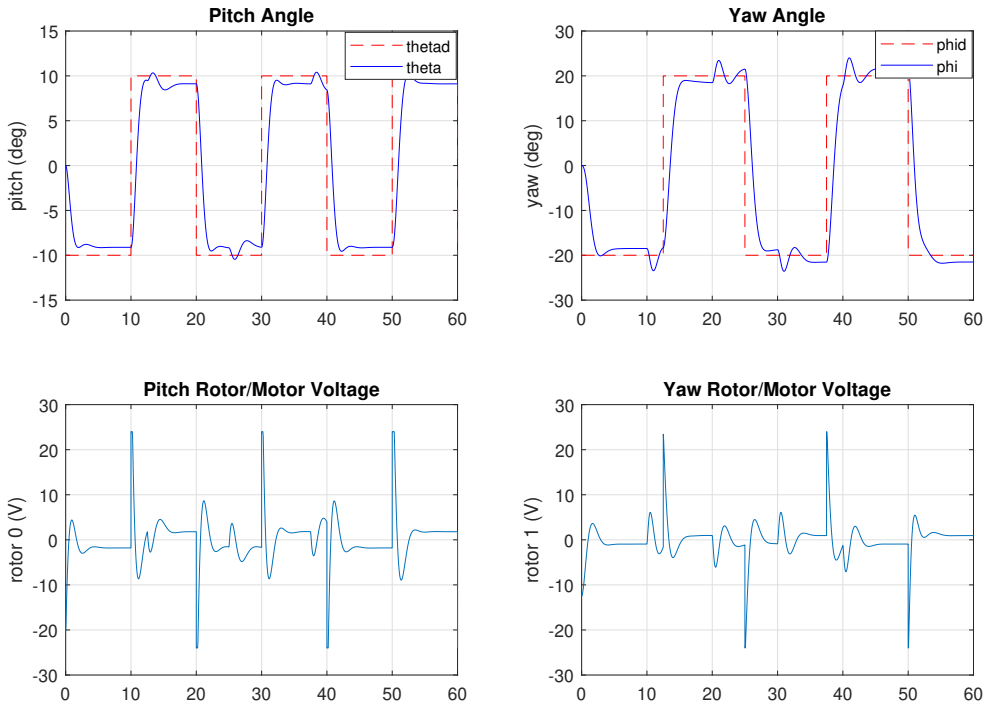

Figure II.4: Simulation results using PD controller for square trajectory tracking

Figure II.4 demonstrate the performance of the PD controller in tracking the desired pitch and yaw angles. The tracking performance indicates that the PD controller regulates the system toward the desired operating point successfully.

The control effort is reflected in the output voltages displayed in Figure II.4. The control effort remains within acceptable limits, ensuring that the motor voltages do not exceed their operational bounds $\pm 24V$.

II.4 Linear Quadratic Regulator design

Linear-Quadratic Regulator (LQR) is a type of optimal control that tries to minimize a quadratic cost function that measures the system's performance and penalizes deviations from desired behavior [25]. In robotics and control systems LQR can be used to design controllers that stabilize the system and track desired trajectories. The LQR controller takes as input the current state of the system, the desired state, and a model of the system dynamics, and computes the optimal control input that minimizes the cost function [25]. Therefore, in the design of the LQR controller for the Quanser Aero2 system, the state-space representation discussed in Section I.4.2.2 is employed.

II.4.1 Controller design

The LQR controller is designed to stabilize the system by determining the optimal control gains based on the state feedback. Figure II.5 depicts the general state-feedback

control using LQR. The state feedback control is defined by:

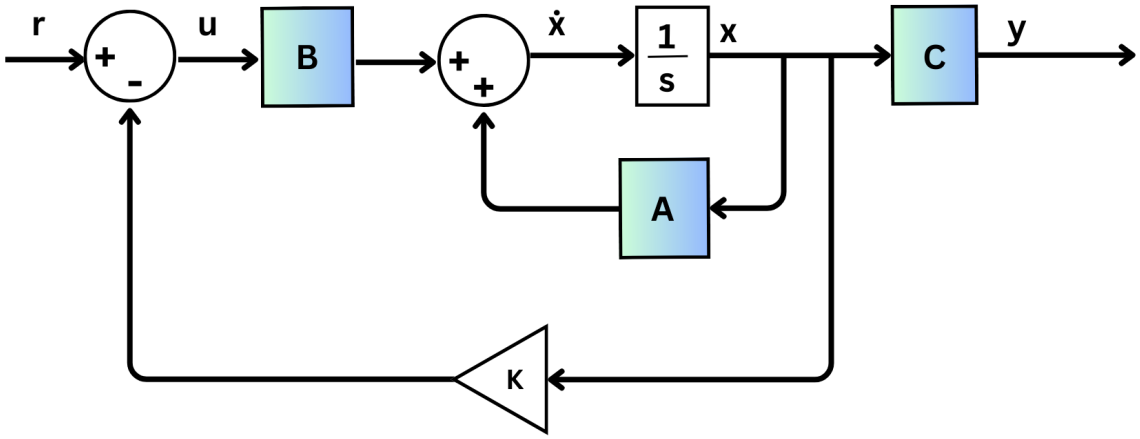

Figure II.5: State-feedback control

$$u = K(x_d - x) \tag{II.14}$$

Where x represents the states that were previously defined in (I.30). Referring to the desired pitch and yaw angles, θ_d and ψ_d, the reference command or setpoint state is defined as:

$$x_d^T = [\theta_d \quad \psi_d \quad 0 \quad 0] \tag{II.15}$$

The control input refers to the voltages of the front/pitch motor and tail/yaw motor, as mentioned in section I.4.2.2 equation (I.31)

The LQR algorithm works by first defining the cost function, which is typically expressed as a weighted sum of the state and control inputs [9]. The weights represent the importance of each term in the cost function and can be adjusted to reflect the desired behavior of the system.

$$J = \int_0^\infty (x_{ref} - x(t))^T Q(x_{ref} - x(t)) + u(t)^T R u(t) dt \tag{II.16}$$

The Q and R matrices are used to impose penalties on deviations of the state variables from their setpoints and on the control actions, respectively. Increasing the value of an element in the Q matrix raises the penalty for any deviations of the associated state variable from its desired setpoint, resulting in a larger specific control gain. On the other hand, boosting the values in the R matrix results in a greater penalty on the aggressiveness of the control action, leading to a uniform decrease in the control gains[21].

Given that there are four states and two control variables, the matrices Q and R have dimensions of $\mathbb{R}^{4\times4}$ and $\mathbb{R}^{2\times2}$, respectively.

The optimal control input, which minimizes the cost function, is determined by using a solution matrix that relates the current state and control inputs of the system.

From this solution matrix, a feedback gain matrix is calculated, which adjusts the system's response to deviations from the desired behavior. With the computed feedback gain matrix, a feedback control law is formulated to stabilize the system around the desired operating point. This control law can be expressed as:

$$u = K(x_d - x) = k_{p,\theta}(\theta_d - \theta) + k_{p,\psi}(\psi_d - \psi) - k_{d,\theta}\dot{\theta} - k_{d,\psi}\dot{\psi} \tag{II.17}$$

By applying this feedback control law, the system is guided towards the desired behavior, minimizing deviations and ensuring stability as intended [21].

II.4.2 Simulation results

The pitch and yaw LQR control of the Aero 2 2 DOF helicopter can be simulated by utilizing the state space representation (I.27) in the following schematic diagram :

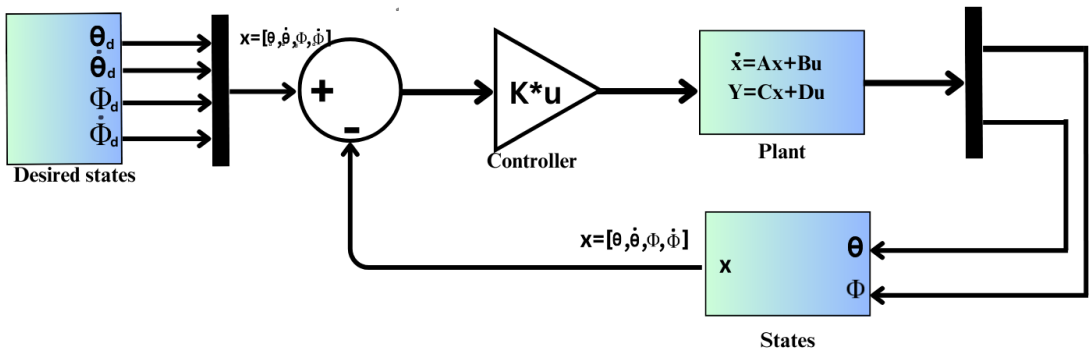

Figure II.6: LQR controller simulation schematic

At the beginning of the simulation, we initialized the Aero2 model with the value 0 to indicate that it was in a resting state. The controller Q and R matrices used in the simulation are:

$$Q = \begin{bmatrix} 150 & 0 & 0 & 0 \\ 0 & 75 & 0 & 0 \\ 0 & 0 & 0 & 0 \\ 0 & 0 & 0 & 0 \end{bmatrix} \qquad R = \begin{bmatrix} 0.01 & 0 \\ 0 & 0.01 \end{bmatrix} \tag{II.18}$$

The Q and R matrices in eq (II.18) are used to compute the gain matrix which is obtained as follows :

$$K = \begin{bmatrix} 99.5844 & -37.6373 & 80.6953 & -24.3159 \\ 47.5974 & 77.9964 & 40.6478 & 52.9117 \end{bmatrix} \tag{II.19}$$

II.4.2.1 Sinusoidal waveform tracking

In this simulation we utilize a sinusoidal function as the desired input signal:

$$\begin{cases} \theta_d = 10 \cdot \sin(2\pi \cdot 0.05 \cdot t) \\ \phi_d = 20 \cdot \sin(2\pi \cdot 0.04 \cdot t) \end{cases} \tag{II.20}$$

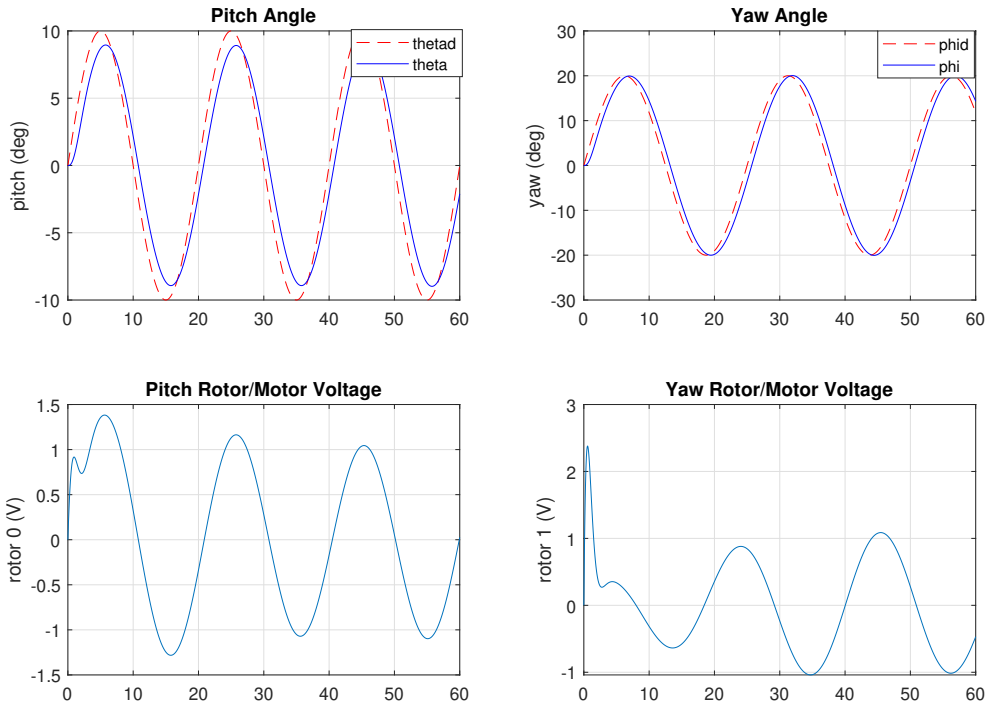

Figure II.7: Simulation results using LQR controller for sinusoidal trajectory tracking

A visual representation of the effectiveness of the Linear Quadratic Regulator (LQR) controller is illustrated in figure III.1. From this figure, we can notice that the actual angle precisely tracks the desired trajectories. Figure III.1 also displays the output voltages that correspond to the control inputs which were within the desired range of $\pm 24V$.

II.4.2.2 Square wave tracking

This simulation utilizes a square function as the desired input signal. The pitch signal oscillates with an amplitude of 10 degrees and a frequency of 0.05 Hertz, while the yaw signal oscillates with an amplitude of 20 degrees and a frequency of 0.04 Hertz. These input signals are utilized to evaluate how accurately the system can track and follow the desired angles.

Figure II.8 shows outputs of the pitch and yaw angles of the Quanser Aero2 system under the LQR controller with the measured voltage at the pitch and yaw motors

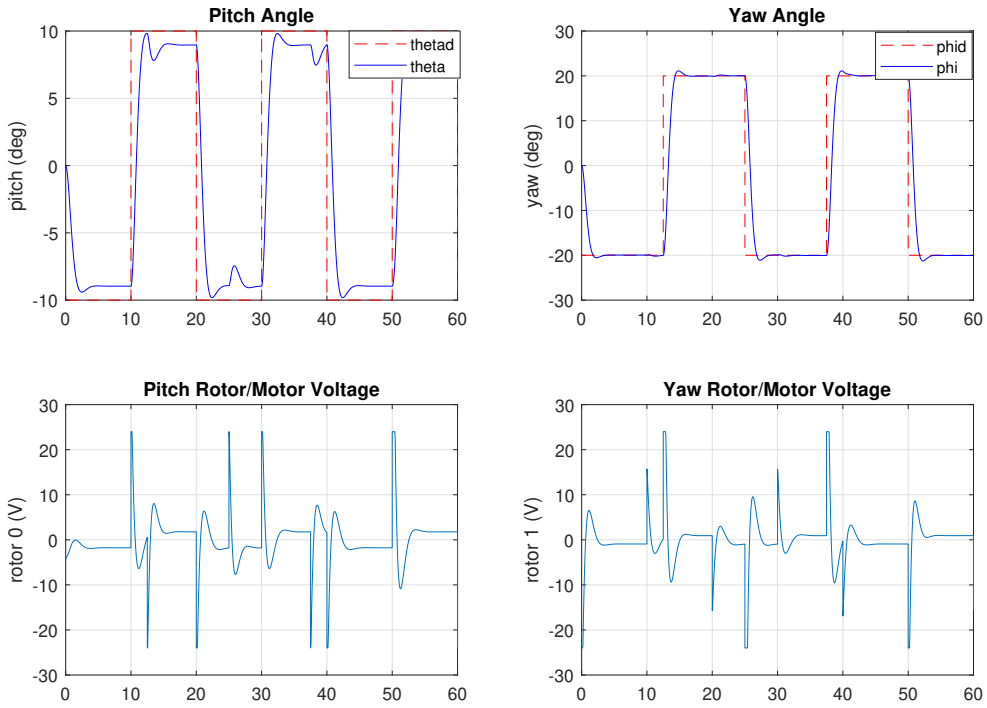

Figure II.8: Simulation results using LQR controller for square trajectory tracking

respectively of the square function. Actual angles precisely follow the desired ones indicating the effectiveness of the LQR controller .

II.5 Sliding Mode Controller

Sliding mode control is a promising approach for dealing with high nonlinearities and parameter fluctuations in control systems, which can improve system stabilization. The fundamental principle of the sliding mode variable structure control involves initially driving the system state and subsequently constraining it within a certain proximity to the switching surface. One of the significant advantages of this approach is that the dynamics of the system can be customized by selecting a suitable switching function, thereby providing robustness to the resulting controllers [26].

II.5.1 Sliding surface choice

In the design of SMC determining the switching surface is an essential phase, which is achieved as the error between the control objectives and reference inputs, along with its derivative. One of the well-applied sliding surfaces was proposed by Slotine [27], which is commonly used in SMC design.

$$S = \left(\frac{d}{dt} + \lambda\right)^{n-1} e \tag{II.21}$$

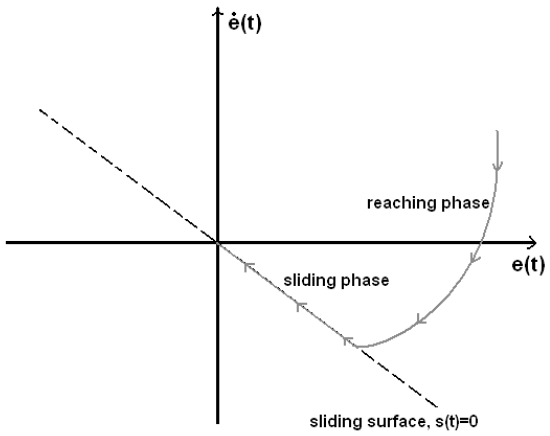

Figure II.9: sliding mode principle of state trajectory

Where : S is the sliding surface, λ is a positive constant and e is the system error and n is the system's relative order.

II.5.2 Existence condition of the sliding mode

To ensure that the system state remains in sliding mode after reaching the sliding surface, it is necessary for the sliding mode to exist at all points of the surface S. Therefore, the existence condition for SMC requires that [28]:

$$\begin{cases} \lim_{s\to 0^-} \dot{S} < 0 \\ \lim_{s\to 0^+} \dot{S} > 0 \end{cases} \tag{II.22}$$

the above expression means that if the sliding surface S is positive, then its derivative should be negative, and if S is negative, then its derivative should be positive. This can be written mathematically as

$$S\dot{S} < 0 \tag{II.23}$$

for all points on the sliding surface.

One can observe that the existence condition presented in (II.23) bears a resemblance to the generalized stability problem. If we define the Lyapunov function V to be [29]:

$$V = \frac{1}{2}S^2 \tag{II.24}$$

Then the existence condition can be summarized in the context of Lyapunov's theory. The goal is to find a suitable control such that $V < 0$. that drives the system states to the sliding surface.

$$\dot{V} = S\dot{S} < 0 \tag{II.25}$$

When the sliding surface $S \neq 0$, $\dot{V}$ is negative definite. Therefore, the condition in (II.25)guarantees that the system asymptotically converges towards the sliding surface and achieves finite-time convergence [30].

II.5.3 Control design

In sliding mode control design, the main challenge is to choose a suitable control law that fulfills the conditions for achieving sliding motion towards the sliding surface while preserving the sliding mode across all points on the surface. To address this issue, the most commonly used control design strategy for robotics is the equivalent control scheme in figure II.10 [27].

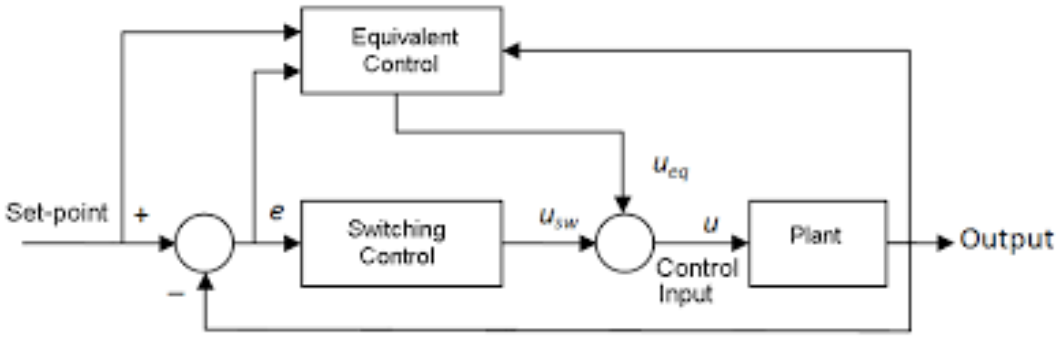

Figure II.10: Equivalent control structure[31].

Sliding mode control design is typically carried out in two parts. The first part involves adding an equivalent control, denoted as U_{eq}, to another control term known as the discontinuous control, denoted as U_n. This is done to ensure that the state trajectory reaches and remains on the switching surface. The control law expression is given by :

$$u = u_{eq} + u_n \tag{II.26}$$

By considering the following state space system:

$$\dot{x}(t) = A(x) + B(x) \tag{II.27}$$

One way to obtain the equivalent control is to realize that in order for the state trajectories to remain on the switching surface $S = 0$, it is necessary that $\dot{S} = 0$ [27]. The time derivative of the sliding surface is given as :

$$\dot{S} = \frac{\partial S}{\partial t} = \frac{\partial S}{\partial x}\frac{\partial x}{\partial t} \tag{II.28}$$

By substituting (II.26) and (II.28) into (II.27):

$$\dot{S} = \frac{\partial S}{\partial x}A(x) + \frac{\partial S}{\partial x}B(x)u_{eq} + \frac{\partial S}{\partial x}B(x)u_n \tag{II.29}$$

During the sliding phase and steady state, the equivalent control is defined such that $s = \dot{S} = 0$ and $u_n = 0$ [30].

$$u_{eq} = -\left(\frac{\partial S}{\partial x}B(x)\right)^{-1}\frac{\partial S}{\partial x}A(x) \tag{II.30}$$

The existence of an inverse matrix is necessary, which leads to the next condition (II.31)

$$\frac{\partial S}{\partial x}B(x) \neq 0 \tag{II.31}$$

By substituting (II.30) in (II.29), the new sliding surface expression becomes:

$$\dot{S} = \frac{\partial S}{\partial x}B(x)u_n \tag{II.32}$$

During the convergence state, the discontinuous control u_n is determined such that it guarantees the finite-time convergence condition $S\dot{S} < 0$ which is given by :

$$S\dot{S} = S\frac{\partial S}{\partial x}B(x)u_n < 0 \tag{II.33}$$

To meet the finite time convergence condition, the sign of the discontinuous control u_n should be opposite to the sign of the expression $S\frac{\partial S}{\partial x}B(x)$. This discontinuous control is typically expressed as a switching term, which is formed by a relay function which is the sign function defined in (II.34) multiplied by a constant gain K.

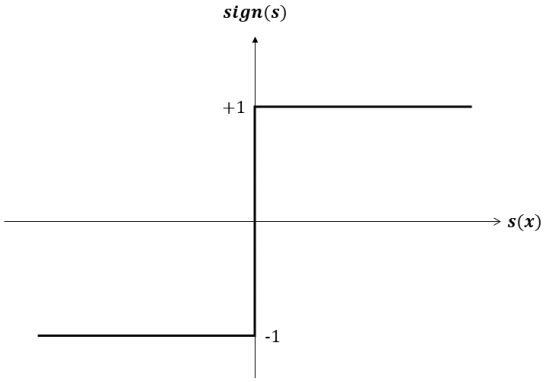

Figure II.11: sign(x) function

$$\text{sign}(s) = \begin{cases} -1, & s < 0 \\ 0, & s = 0 \\ +1, & s > 0 \end{cases} \tag{II.34}$$

Then the discontinuous control law is given by:

$$u_n = -K\,\text{sign}(s) \tag{II.35}$$

The coefficient K must be positive to ensure the convergence condition.

II.5.4 SM controller design for Quanser Aero2

In this section, we will introduce the design of sliding mode controller for the Quanser Aero2 Experiment. The equations of motion for the system are presented in section I.4.1, with the pitch equation given by (I.16). To simplify notation, we can express it as follows:

$$\ddot{\theta} = A_1 + B_{11}V_p + B_{12}V_y \tag{II.36}$$

and the yaw equation given by (I.17) as :

$$\ddot{\psi} = A_2 + B_{21}V_p + B_{22}V_y \tag{II.37}$$

where : $B_{11} = \frac{D_t K_{pp}}{a}$, $B_{12} = \frac{D_t K_{py}}{a}$, $B_{21} = \frac{D_t K_{yp}}{b}$, $B_{22} = \frac{D_t K_{yy}}{b}$
and $A_1 = \frac{-mgl_{cm}\cos\theta - D_p\dot{\theta} - ml_{cm}^2\sin\theta\cos\theta\dot{\psi}^2}{a}$, $A_2 = \frac{2ml_{cm}^2\sin\theta\cos\theta\dot{\theta}\dot{\psi} - D_y\dot{\psi}}{b}$
Taking the sliding surface for the setpoint tracking as [32]:

$$[s] = \begin{bmatrix} s_p \\ s_y \end{bmatrix} = \begin{bmatrix} \dot{e}_p + c_p e_p \\ \dot{e}_y + c_y e_y \end{bmatrix} \tag{II.38}$$

where c_p, c_y will satisfy Hurwitz condition, and $c_p > 0$, $c_y > 0$, e_p and e_y are the errors for pitch and yaw respectively, and defined as:

$$e_p = \theta - \theta_{\text{desired}} \tag{II.39}$$

$$e_y = \psi - \psi_{\text{desired}} \tag{II.40}$$

Taking the time derivative of sliding surface:

$$[\dot{s}] = \begin{bmatrix} \ddot{\theta} + c_p\dot{\theta} \\ \ddot{\psi} + c_y\dot{\psi} \end{bmatrix} \tag{II.41}$$

$$= \begin{bmatrix} A1 + B11Vp + B12Vy + c_p\dot{\theta} \\ A2 + B21Vp + B22Vy + c_y\dot{\psi} \end{bmatrix} \tag{II.42}$$

$$= \begin{bmatrix} A_1 \\ A_2 \end{bmatrix} + \begin{bmatrix} B_{11} & B_{12} \\ B_{21} & B_{22} \end{bmatrix} \begin{bmatrix} V_p \\ V_y \end{bmatrix} + \begin{bmatrix} c_p\dot{\theta} \\ c_y\dot{\psi} \end{bmatrix} \tag{II.43}$$

The exponential reaching law [33] is utilized in the design of the control law for SMC. It is expressed as:

$$[\dot{s}] = -\begin{bmatrix} k_1\,\text{sign}(s_p) + k_3 s_p \\ k_2\,\text{sign}(s_y) + k_4 s_y \end{bmatrix} \tag{II.44}$$

The first term in the exponential reaching law is used to ensure faster convergence when the errors are small, while the second term (proportional term) forces the states

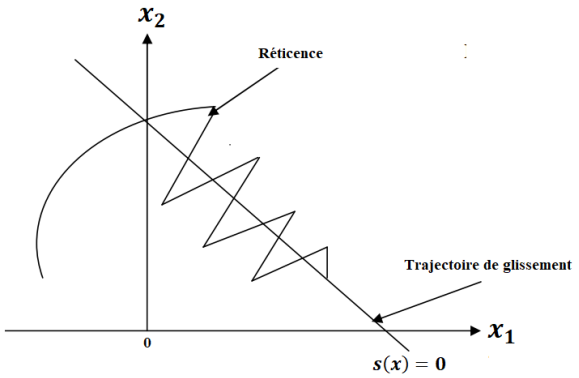

Figure II.12: The chattering phenomena

to reach the switching surface more quickly when the errors are large. After solving equation (II.43) and (II.48) , we obtain the control inputs as:

$$\begin{bmatrix} V_p \\ V_y \end{bmatrix} = - \begin{bmatrix} B_1 & B_{12} \\ B_{21} & B_2 \end{bmatrix}^{-1} \begin{bmatrix} A_1 + c_p\dot{\theta} + k_1 \operatorname{sign}(s_1) + k_3 s_p \\ A_2 + c_y\dot{\psi} + k_2 \operatorname{sign}(s_y) + k_4 s_y \end{bmatrix} \tag{II.45}$$

In the control of dynamic systems, the use of SMC can be advantageous because it provides robustness against disturbances and uncertainties. However, a common problem associated with SMC is chattering.

II.5.5 Chattering phenomenon

Chattering phenomenon is a well-known problem associated with SMC and has been extensively studied in the literature. According to Levant [26], chattering is an undesirable behavior that results in high-frequency oscillations in the control signal due to the discontinuous nature of the control law.

Several techniques have been proposed to mitigate chattering in SMC, the most common one is to replace the classical $sign(x)$ function with a smoother switching function, such as saturation function $sat(x)$ and hyperbolic tangent function $tanh(x)$[34]. as shown in Figure II.13

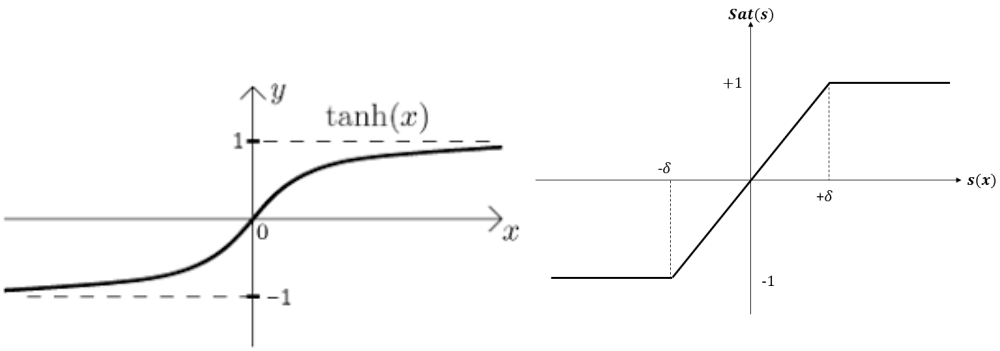

(a) tanh(x) (b) sat(x)

Figure II.13: tangent hyperbolic and saturation functions

The shown functions are defined by:

$$sat(x) = \begin{cases} a, & \text{if } x < a \\ x, & \text{if } a \leq x \leq b \\ b, & \text{if } x > b \end{cases} \tag{II.46}$$

$$sigm(x) = -1 + \frac{2}{1 + e^{-ax}} \tag{II.47}$$

To attenuate chattering of the SMC controller for the Quanser aero2, we have used the hyperbolic tangent (tanh) function. Then the exponential reaching law that is utilized in the design of the control law for SMC becomes:

$$[\dot{s}] = -\begin{bmatrix} k_1 \tanh(s_p) + k_3 s_p \\ k_2 \tanh(s_y) + k_4 s_y \end{bmatrix} \tag{II.48}$$

and the control inputs become:

$$\begin{bmatrix} V_p \\ V_y \end{bmatrix} = -\begin{bmatrix} B_1 & B_{12} \\ B_{21} & B_2 \end{bmatrix}^{-1} \begin{bmatrix} A_1 + c_p\dot{\theta} + k_1 \tanh(s_p) + k_3 s_p \\ A_2 + c_y\dot{\psi} + k_2 \tanh(s_y) + k_4 s_y \end{bmatrix} \tag{II.49}$$

II.5.6 Stability of sliding mode controller

In order to assess the stability of a 2-DOF helicopter that is controlled by a sliding mode controller, the Lyapunov method is employed. This method is widely used in control theory to verify the stability of a system by analyzing a suitable Lyapunov function. In this case, a Lyapunov candidate function is selected to be quadratic in terms of the pitch and yaw surfaces [35].

$$V(s_\theta, s_\psi) = \frac{1}{2}(s_\theta^2 + s_\psi^2) \tag{II.50}$$

The time derivative of the Lyapunov function can be computed as

$$\dot{V} = s_\theta(\dot{s}_\theta) + s_\psi(\dot{s}_\psi) \tag{II.51}$$

Using equation II.48, it becomes:

$$\dot{V} = s_\theta(-k_1 \text{sign}(s_\theta) - k_2 s_\theta) + s_\psi(-k_3 \text{sign}(s_\psi) - k_4 s_\psi) \tag{II.52}$$

$$\dot{V} \leq -k_1 |s_\theta| - k_2 s_\theta^2 - k_3 \left|s_\phi\right| - k_4 s_\phi^2 \tag{II.53}$$

In order to ensure the stability of the 2-DOF helicopter, the values of k_1, k_2, k_3 and k_4 must be strictly greater than zero . It is clear that V is positive definite, and from the derived inequality, we can observe that $\dot{V}$ is always negative or zero. For stability analysis, it is desirable to have a negative definite $\dot{V}$. However, the presence of zero

indicates that the system can reach a sliding mode, where the motion along the sliding surface (represented by s_θ and s_ϕ) can be maintained.

II.5.7 Simulation results

The pitch and yaw SM control of the Aero 2 2-DOF helicopter can be simulated utilizing the nonlinear model given by (I.16) and (I.17) along with the sliding surface (II.38) and control laws to define the control inputs as (II.49) as illustrated in the following schematic diagram:

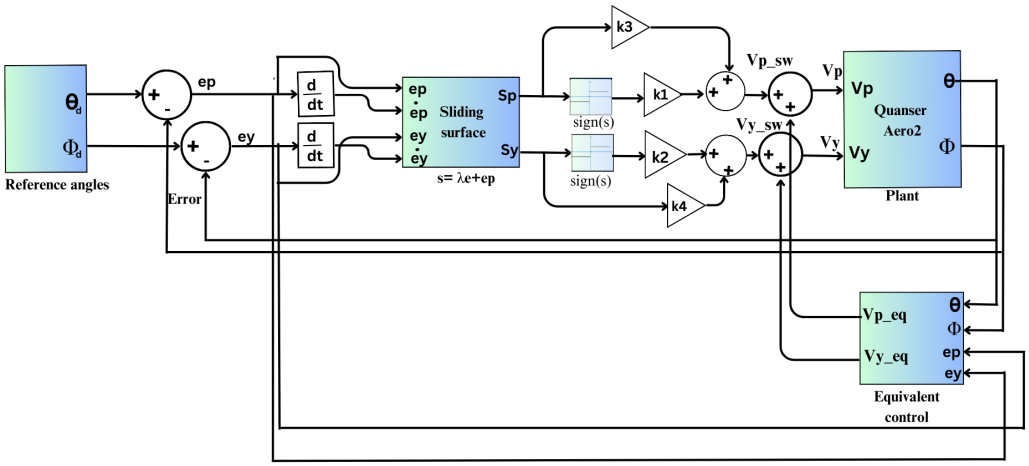

Figure II.14: SM controller simulation schematic

The initial conditions of the Aero2 model were configured as 0 to describe its state of rest at the start of the simulation.

II.5.7.1 Sinusoidal waveform tracking

To test the tracking performance of the system, this simulation incorporates a sinusoidal function as the desired input signal.

$$\begin{cases} \theta_d = 10 \cdot \sin(2\pi \cdot 0.05 \cdot t) \\ \phi_d = 20 \cdot \sin(2\pi \cdot 0.04 \cdot t) \end{cases} \tag{II.54}$$

The controller gains used in the simulation are listed in Table II.2:

Pitch	c_p=10	k_1=50	k_2=6
Yaw	c_y=10	k_3=100	k_4=20

Table II.2: The controller gains for the sinusoidal waveform simulation using SMC

Figure II.78 shows the SM controller's performance in tracking the desired pitch and yaw angles of the Quanser Aero2 system. It exhibits precise and stable control,

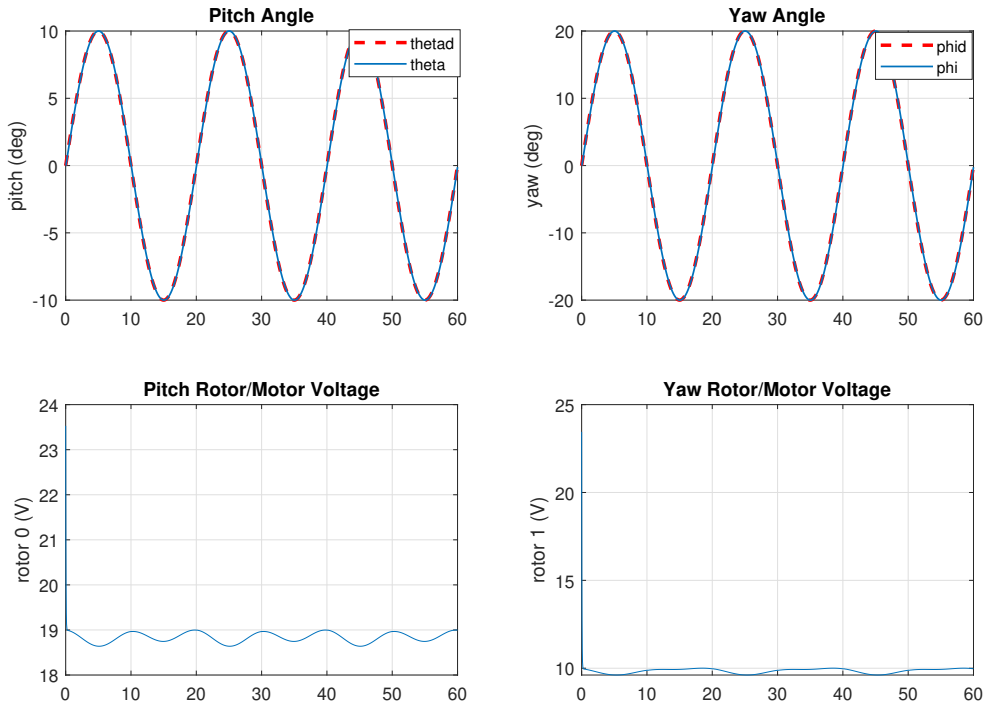

Figure II.15: Simulation results using SM controller for sinusoidal trajectory tracking

outperforming the PD and LQR controllers.That was after successfully mitigating the chattering due to the use of the hyperbolic tangent function in the controller instead of the original sign function as defined in the control inputs(II.49) . The control effort generated by the SM controller is also depicted in figure II.78 by the output pitch and yaw motors respectively, the control action is smoother than that of the LQR and PD controllers ,it stays within the required limits of $\pm 24V$

II.5.7.2 Square wave tracking

In order to evaluate the system's ability to track desired signals, this simulation employs a square function as the input signal. The pitch signal has a frequency of 0.05 Hertz and an amplitude of 10 degrees, while the yaw signal has a frequency of 0.04 Hertz and an amplitude of 20 degrees. The controller gains used in the simulation are listed in Table II.3:

Pitch	c_p=10	k_1=3	k_2=0.3
Yaw	c_y=10	k_3=10	k_4=5

Table II.3: The controller gains for the square wave simulation using SMC

Figure II.16 demonstrate the output pitch and yaw angles of the Quanser Aero2 system under the SM controller, along with the measured voltage at the pitch and

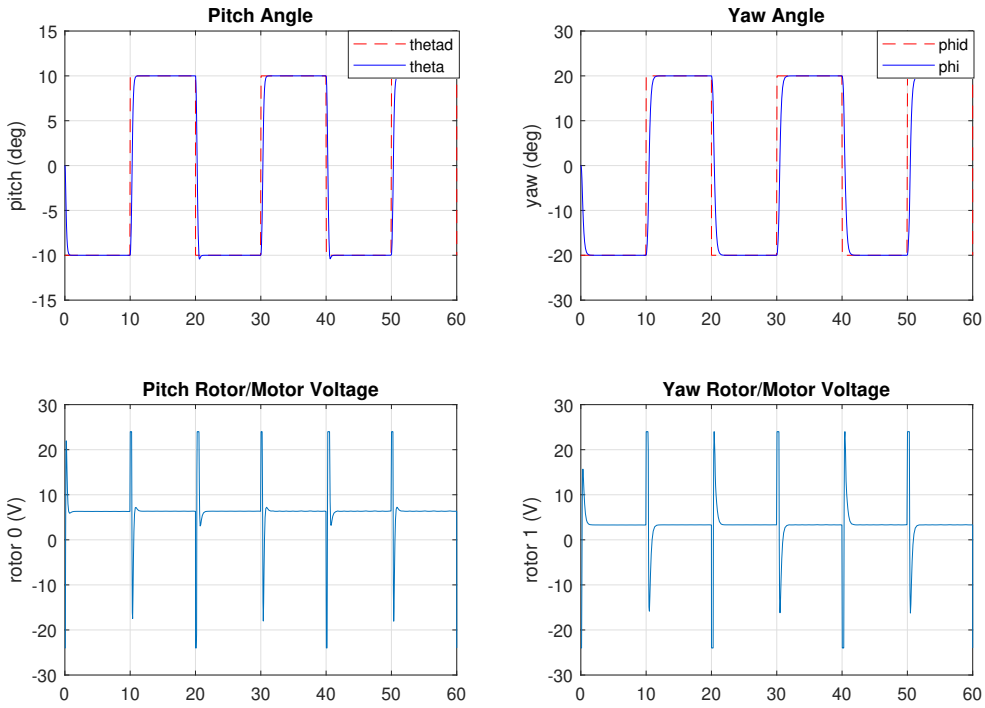

Figure II.16: Simulation results using SM controller for square trajectory tracking

yaw motors, respectively, when subjected to a square function input We can notice that chattering has been effectively mitigated due to the use of the hyperbolic tangent function as defined in the control inputs(II.49). The SM controller shows enhanced performance than that of the linear controllers by accurately tracking the desired angles.

II.6 Super-twisting controller

The Super Twisting Controller (STC) has gained significant attention as a prominent high-order sliding mode control technique it is the second order sliding mode control to be more specific introduced to effectively addresses a common limitation in the standard sliding mode control: chattering. That, solves this issue by introducing a higher-order sliding surface and a nonlinear switching term which facilitates rapid convergence[36].

In this section, the Super Twisting Controller will be introduced, including its mathematical formulation and design considerations specific to the 2-DOF Quanser Aero 2 helicopter system.

II.6.1 Controller design for Quanser Aero2

The design of the super-twisting controller for the Quanser Aero2 system involved the utilization of the linear model for the pitch (I.28) and yaw (I.29).

First, the sliding mode control design is established for pitch channel with θ signal. The sliding surface similar to the sliding mode control is given by:

$$s_\theta = e_\theta + c_p e_\theta \tag{II.55}$$

Here, the parameter c_p is a positive value chosen during the design process, and e_θ represents the difference between the desired angular position (θ_d) and the actual position (θ). This error term quantifies the deviation between the desired and actual positions of the system.

$$e_\theta = \theta_d - \theta \tag{II.56}$$

The time derivative of equation (II.55) gives:

$$\dot{s_\theta} = \dot{e_\theta} + c_p \dot{e_\theta} = \ddot{\theta_d} - \dot{\theta} + c_p \dot{e_\theta} \tag{II.57}$$

Substituting in (I.28), the following is obtained[37]:

$$\dot{s_\theta} = \ddot{\theta_d} - \frac{Dt * Kpp * Vp + Dt * Kpy * Vy - Dp * \dot{\theta}}{Jp} + c_p \dot{e_\theta} \tag{II.58}$$

The pitch control signal consists of equivalent and switching control laws as follows:

$$V_p = \left(\frac{Jp}{Dt * Kpp}\right)(u_{eq} + u_{sw}) \tag{II.59}$$

The equivalent control law can be defined as:

$$u_{eq1} = \ddot{\theta_d} - \left(\frac{Dt * Kpy}{Jp}\right) V_y + \left(\frac{Dp}{Jp}\right) \dot{\theta} + c_p \dot{e_\theta} \tag{II.60}$$

On the other hand, the switching control law is designed based on the super twisting algorithm. The switching control law is set as follows[37]:

$$u_{sw1} = k1\sqrt{|s_\theta|}sgn(s_\theta) + k2 \int sgn(s_\theta)dt \tag{II.61}$$

where k_1 and k_2 are positive design parameters. Substituting (II.60) and (II.61) into (II.59), the following is obtained:

$$V_p = \left(\frac{Jp}{D_t * Kpp}\right)\left(\ddot{\theta_d} - \left(\frac{D_t * K_{py}}{J_p}\right) V_y + \left(\frac{D_p}{J_p}\right) \dot{\theta} + c_p \dot{e_\theta} + k_1\sqrt{|s_\theta|}sgn(s_\theta) + k_2 \int sgn(s_\theta)dt\right) \tag{II.62}$$

Then, substituting (II.62) into (II.58), we obtain:

$$\dot{s_\theta} = -k_1\sqrt{|s_\theta|}sgn(s_\theta) - k_2 \int sgn(s_\theta)dt \tag{II.63}$$

To design the controller for the ψ signal the same principle is followed. The sliding surface is chosen as follows:

$$s_\psi = e_\psi + c_y e_\psi \tag{II.64}$$

Where c_y is a positive design parameter,and e_ψ denotes the error between the desired angular position (ψ_d) and the actual position (ψ).

$$e_\psi = \psi_d - \psi \tag{II.65}$$

Taking the time derivative of the sliding surface equation to have:

$$\dot{s_\psi} = \dot{e_\psi} + c_y \dot{e_\psi} = \ddot{\psi}_d - \dot{\psi} + c_y \dot{e_\psi} \tag{II.66}$$

Using eq (I.29) , (II.66) becomes:

$$\dot{s_\psi} = \ddot{\psi}_d - \frac{D_t * K_{yp} * V_p + D_t * K_{yy} * V_y - D_y * \dot{\psi}}{Jy} + c_y \dot{e_\psi} \tag{II.67}$$

substituting equation (II.62) into equation (II.67) , the following is obtained :

$$\begin{aligned}\dot{s_\psi} = \ddot{\psi}_d - \frac{K_{yp}J_p}{K_{pp}J_y}\left(\ddot{\theta}_d - \left(\frac{D_t K_{py}}{J_p}\right)V_y + \left(\frac{D_p}{J_p}\right)\dot{\theta} + c_1\dot{e_\theta} + \sqrt{|s_\theta|}sgn(s_\theta) + k_2\int sgn(s_\theta)dt\right) \\ - \left(\frac{K_{yy}}{J_y}\right)V_y + \left(\frac{D_y}{J_y}\right)\dot{\psi} + c_2\dot{e_\psi}\end{aligned} \tag{II.68}$$

The yaw control signal V_y is also composed of two components: equivalent and switching control laws. Therefore, this yaw control signal is defined by [37]:

$$V_y = \frac{J_y K_{pp}}{D_t(K_{yy}K_{pp} + K_{yp}K_{py})}(u_{eq2} + u_{sw2}) \tag{II.69}$$

The equivalent control law is assigned as:

$$\begin{aligned}u_{eq2} = \ddot{\psi}_d - \left(\frac{K_{yp}J_p}{J_y K_{pp}}\right)\ddot{\theta}_d - \left(\frac{K_{yp}D_p}{J_y K_{pp}}\right)\dot{\theta}_d - \left(\frac{K_{yp}J_p c_p}{J_y K_{pp}}\right)\dot{e_\theta} - \left(\frac{K_{yp}J_p}{J_y K_{pp}}k_1\sqrt{|s_\theta|}\right) \\ \text{sgn}(s_\theta) - \left(\frac{K_{yp}J_p}{J_y K_{pp}}k_2\right)\int \text{sgn}(s_\theta)\,dt + \left(\frac{D_y}{J_y}\right)\dot{\psi} + c_y\dot{e_\psi}.\end{aligned} \tag{II.70}$$

The switching control law component is given by :

$$u_{sw2} = k_3\sqrt{|s_\psi|}sgn(s_\psi) + k_4\int sgn(s_\psi)dt \tag{II.71}$$

By considering positive design parameters k_3 and k_4, and substituting eq (II.70) and (II.71) into eq (II.69), the resulting expression is as follows:

$$V_y = \frac{J_y K_{pp}}{D_t(K_{yy}K_{pp}+K_{yp}K_{py})}\left(\ddot{\psi}_d - \left(\frac{K_{yp}J_p}{J_y K_{pp}}\right)\ddot{\theta}_d - \left(\frac{K_{yp}D_p}{J_y K_{pp}}\right)\dot{\theta}_d - \left(\frac{K_{yp}J_p c_p}{J_y K_{pp}}\right)\dot{e_\theta} - \left(\frac{K_{yp}J_p}{J_y K_{pp}}k_1\sqrt{|s_\theta|}\right) \times \mathrm{sgn}(s_\theta) - \left(\frac{K_{yp}J_p}{J_y K_{pp}}k_2\right)\int \mathrm{sgn}(s_\theta)dt + \left(\frac{D_y}{J_y}\right)\dot{\psi} + c_y\dot{e_\psi} + k_3\sqrt{|s_\psi|}\mathrm{sgn}(s_\psi) + k_4\int \mathrm{sgn}(s_\psi)dt\right). \tag{II.72}$$

Substituting (II.72) into (II.68), $\dot{s_\psi}$ reduces as follows:

$$\dot{s_\psi} = -k_3\sqrt{|s_\psi|}sgn(s_\psi) - k_4\int sgn(s_\psi)dt \tag{II.73}$$

II.6.2 Stability of super-twisting controller

The stability analysis of the 2-DOF helicopter system controlled by the super-twisting controller involves the application of the Lyapunov method [35].

$$V(s_\theta, s_\psi) = \frac{1}{2}(s_\theta^2 + s_\psi^2) \tag{II.74}$$

The time derivative of the Lyapunov function can be computed as

$$\dot{V} = s_\theta(\dot{s_\theta}) + s_\psi(\dot{s_\psi}) \tag{II.75}$$

Using eq (II.63) and (II.73) it becomes:

$$\dot{V} = s_\theta\left(-k_1\sqrt{|s_\theta|}sgn(s_\theta) - k_2\int sgn(s_\theta)dt\right) + s_\psi\left(-k_3\sqrt{|s_\psi|}sgn(s_\psi) - k_4\int sgn(s_\psi)dt\right) \tag{II.76}$$

$$\dot{V} \leq -k_1\sqrt{|s_\theta|}s_\theta - |s_\theta|\int k_2 dt - k_3\sqrt{|s_\psi|}s_\psi - |s_\psi|\int k_4 dt \tag{II.77}$$

In this inequality, k_1, k_2, k_3, and k_4 are positive design parameters. The condition $\dot{V} \leq 0$ indicates that V is a decreasing function over time. By selecting appropriate values for k_1, k_2, k_3, and k_4, the inequality can be satisfied, ensuring the stability of the system. Specifically, the terms involving the sliding variables s_θ and s_ψ, as well as their integrals, contribute to the stability analysis [26].

II.6.3 Simulation results

The pitch and yaw super-twisting control of the Aero 2 2 DOF helicopter can be simulated utilizing the linear model of the system (I.28)and (I.29) with the sliding surface and control inputs (II.62), (II.72). These are illustrated in the following schematic diagram :

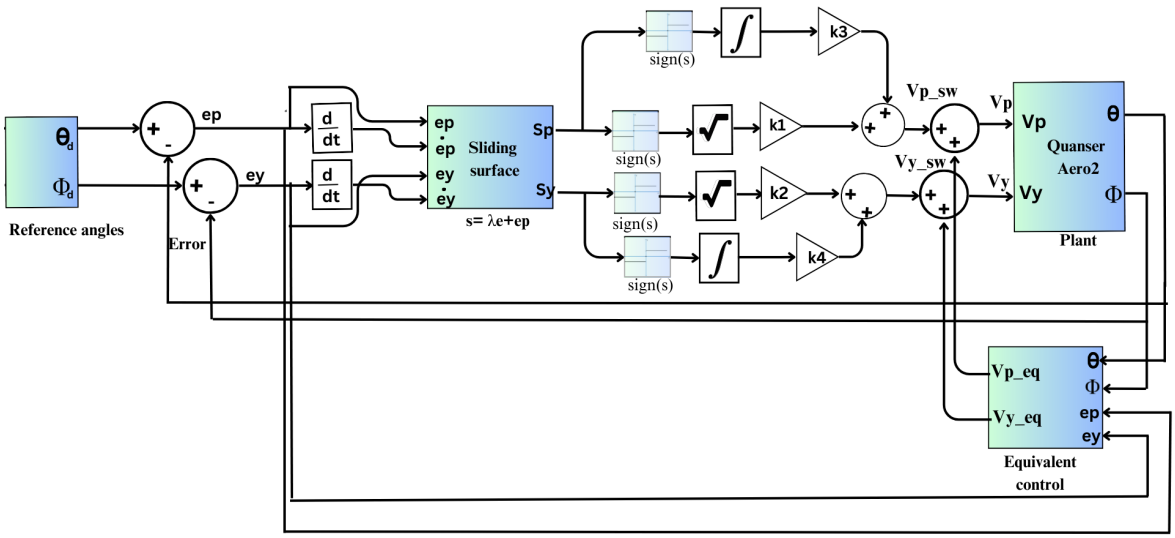

Figure II.17: Super-twisting controller simulation schematic

II.6.3.1 Sinusoidal waveform tracking

In this simulation, we use a sinusoidal function as the input signal to see how well the system can follow and track it.

$$\begin{cases} \theta_d = 10 \cdot \sin(2\pi \cdot 0.05 \cdot t) \\ \phi_d = 20 \cdot \sin(2\pi \cdot 0.04 \cdot t) \end{cases} \tag{II.78}$$

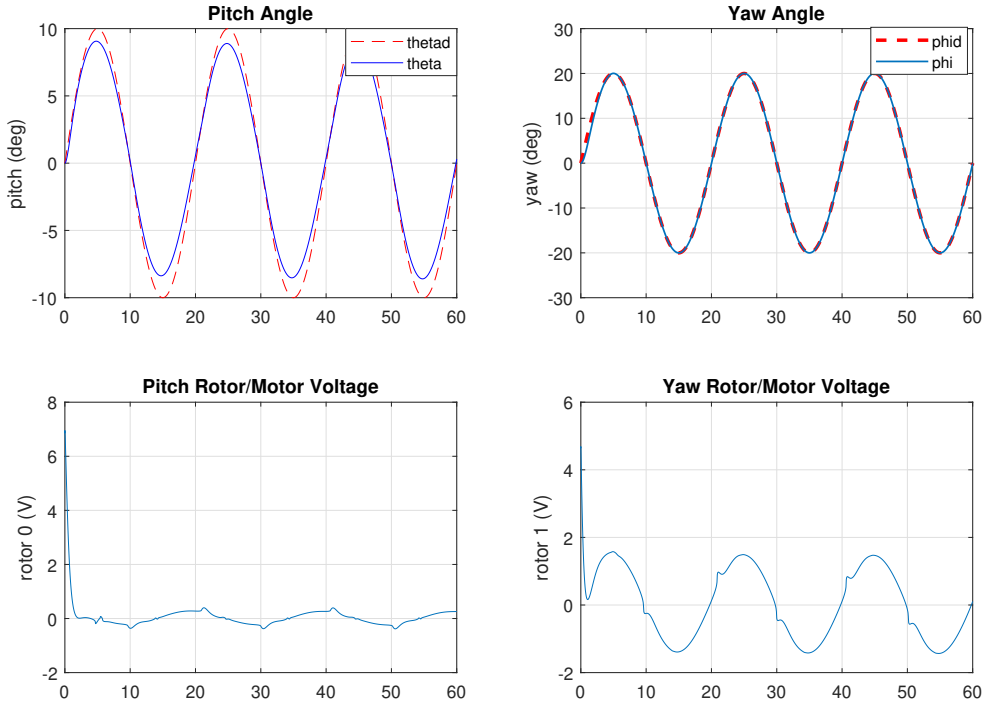

Figure II.18: Simulation results using ST controller for sinusoidal trajectory tracking

The controller gains used in the simulation are listed in Table II.4:

Pitch	c_p=190000	k_1=55	k_2=145
Yaw	c_y=8999990000	k_3=100000	k_4=80000

Table II.4: The controller gains for the sinusoidal waveform simulation using STC

Figure II.18 shows the output pitch and yaw angles of the Quanser Aero2 system controlled by the ST controller. The figure also includes the corresponding measured voltage at the pitch and yaw motors, providing a comprehensive overview of the system's behavior where it accurately tracks the desired angles exibiting smooth limited control actions.

II.6.3.2 Square wave tracking

To evaluate the system's tracking capabilities, the simulation employs a square function as the desired input signal. The pitch signal is characterized by an amplitude of 10 degrees and a frequency of 0.05 Hertz, while the yaw signal has an amplitude of 20 degrees and a frequency of 0.04 Hertz.

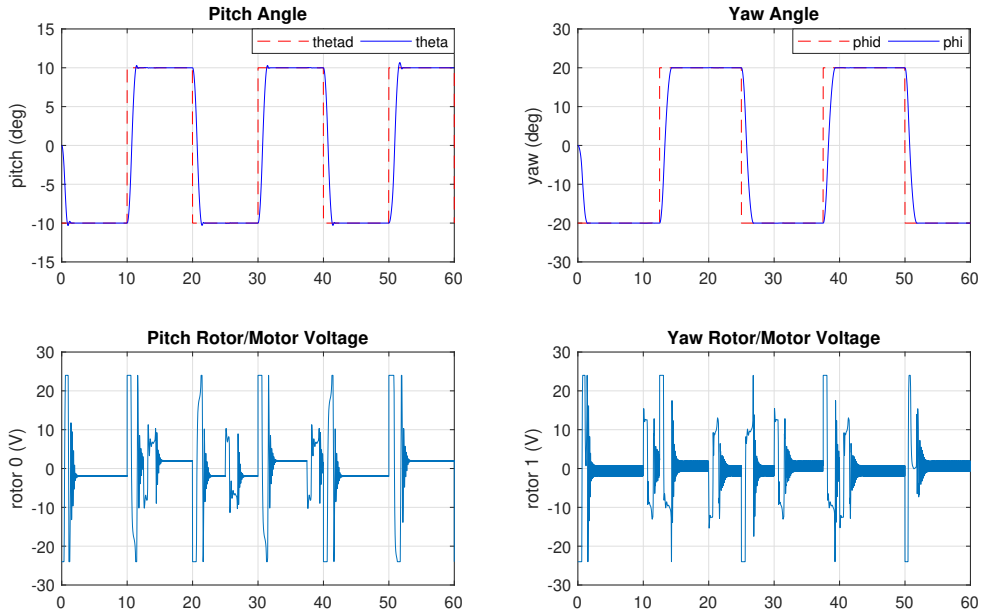

Figure II.19: Simulation results using ST controller for square trajectory tracking

The controller gains used in the simulation are listed in Table II.5:

Figure II.19 presents the output pitch and yaw angles of the Quanser Aero2 system under the control of the ST controller when subjected to a square function which visually illustrate the convergence of the actual angles towards the desired angles effectively . The figure also includes the measured voltage at the pitch and yaw motors.

Pitch	$c_p = 10^6$	$k_1 = 1000$	$k_2 = 10$
Yaw	$c_y = 9x10^{10}$	$k_3 = 10^5$	$k_4 = 10$

Table II.5: The controller gains for the square wave simulation using STC

II.7 Comparative analysis of the simulation results

In this section a comparison between the four controllers is held first by visual inspection of the output graphs illustrated in Figure II.20 of the PD, LQR , SM and ST controllers respectively , we can note that the PD controller demonstrates satisfactory performance in regulating the output angles, although it exhibits some steady-state error. On the other hand, the LQR controller exhibits superior performance with reduced steady-state error , thanks to its optimal control design. However, it requires accurate knowledge of the system model. The SM and ST controllers exhibit even enhanced performance in achieving accurate tracking of the desired angles. They demonstrate robust performance.

For a more accurate comparison of these results, we can use the performance metrics that are demonstrated in Tables II.6 and II.7 :

Response Results	PD controller	LQR controller	SM controller	ST controller
Square wave				
Overshoot ($PO\%$)	5.27	4.807	**0.505**	2.419
Peak time t_p	3	3	**1**	2
Rise time t_r	1.163	1.164	**0.391**	0.816
Sinusoidal waveform				
Root mean square error	6.662	6.232	7.262	**6.129**

Table II.6: Simulated response results for the pitch signal

Response results	**PD controller**	**LQR controller**	**SM controller**	**ST controller**
Square wave				
Overshoot ($PO\%$)	5.47	2.63	**0.504**	0.505
Peak time t_p	2	2	**1**	2
Rise time t_r	2.203	1.112	**0.580**	1.042
Sinusoidal waveform				
Root mean square error	14.27	14.29	14.52	**14.10**

Table II.7: Simulated response results for the yaw signal

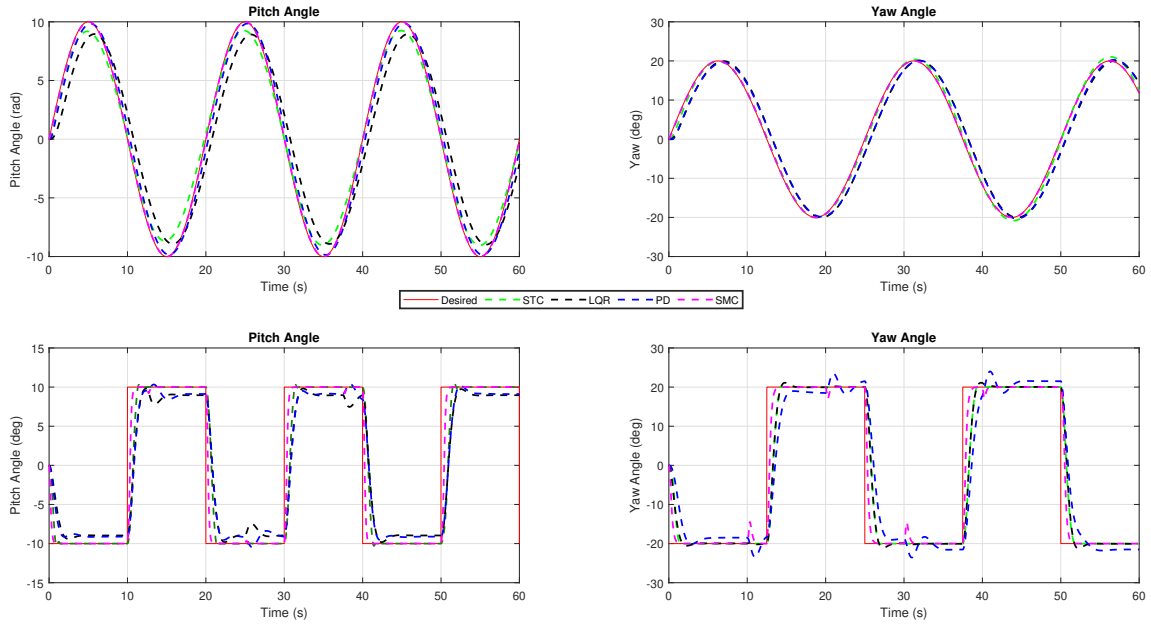

Figure II.20: Comparison of the simulation results

Among the four controllers evaluated in the simulation, namely the PD, LQR, SM, and ST controllers, the overshoot and rise time performances vary.

In terms of overshoot for the square wave tracking, the PD controller exhibits the highest overshoot with value of $PO = 5.47\%$ and $PO = 5.27\%$ for the yaw and pitch signals respectively . The LQR controller performs slightly better with reduced overshoot. The SM controller shows a significant reduction in overshoot, achieving values of 0.505% and 0.504% for the pitch and yaw signals respectively. The ST controller achieves well in terms of overshoot values of 2.419% for the pitch signal and an impressive 0.505% for the yaw signal.

Moving on to the rise time the square wave tracking, the PD controller has the longest rise time with values of $t_r = 2.203s$ and $t_r = 1.163s$ for the yaw and pitch signals respectively. The LQR controller performs slightly better. However, The SM controller demonstrates a significant improvement, achieving rise times of 0.391 for the pitch signal and 0.580 for the yaw signal. The ST controller performs well in terms of rise time as well.

For the root mean square error of the sinusoidal waveform tracking the SM controller exhibits the highest root mean square error of values 7.262 and 14.52 for the pitch and yaw angles respectively the PD and LQR exhibit enhanced results with lower error , the ST controller exhibits even better results in terms of root mean square error with values of 6.129 and 14.10 for the pitch and yaw signals respectively.

Considering both overshoot and rise time,peak time annd root mean square error it is evident that the SM and ST controllers outperform the PD and LQR controllers. The SM and ST controllers achieve notably lower overshoot values and faster rise times compared to the PD and LQR controllers.Therefore, based on these performance

metrics, the ST and SM controllers can be considered the superior controllers among the four evaluated in terms of achieving accurate and stable control performance.

II.8 Conclusion

This chapter has covered the design procedures for four different control strategies to achieve trajectory tracking of the Quanser Aero 2 2-DOF helicopter. Then, we have simulate these controllers by introducing a sinusoidal waveform and a square wave to evaluate their performance with a comparative analysis for the results obtained. Moving forward, the next chapter will focus on the real-time implementation of these controllers on the Quanser Aero2 platform.

Chapter III

Real-time implementation of the controllers

III.1 Introduction

In this chapter the focus is on the practical realization of the control strategies (PD, LQR, SMC and STC) using the Quanser Aero2 platform in the Control Laboratory of the Center of Developement of Advanced Technologies (CDTA). This chapter provides the hardware setup, software development, and integration of the control algorithms with the physical system. Performance evaluation and comparison of the implemented controllers are conducted using various metrics to assess their tracking accuracy, precision and robustness.

III.2 QUARC Real-Time Control software

QUARC (Quanser Real-Time Control) is a software package developed by Quanser [38], specifically designed for real-time control and implementation of Quanser systems. It provides a comprehensive set of tools, libraries, and APIs (Application Programming Interfaces) that enable users to interface with Quanser hardware and develop real-time control algorithms. This streamlined approach is primarily used in conjunction with MATLAB and Simulink, allowing users to design control algorithms in Simulink and deploy them onto Quanser hardware platforms for real-time control.

QUARC facilitates the transition of Simulink designs into real-time applications by directly generating real-time code from Simulink-designed controllers. With the ability to execute code in real-time on Windows targets, by providing the necessary drivers and communication protocols, QUARC ensures reliable and accurate real-time control implementation for Quanser systems [38]. Figure III.1 shows the Simulink model that is used with QUARC to run the LQR-based state-feedback control on the Aero 2.

The Simulink model uses specific blocks namely the HIL Write Analog and HIL Read Time-base from the QUARC Targets library to control input voltage to the rotors and measure the corresponding pitch and yaw responses. These responses are saved into a MATLAB *.mat file using the To Host File block.

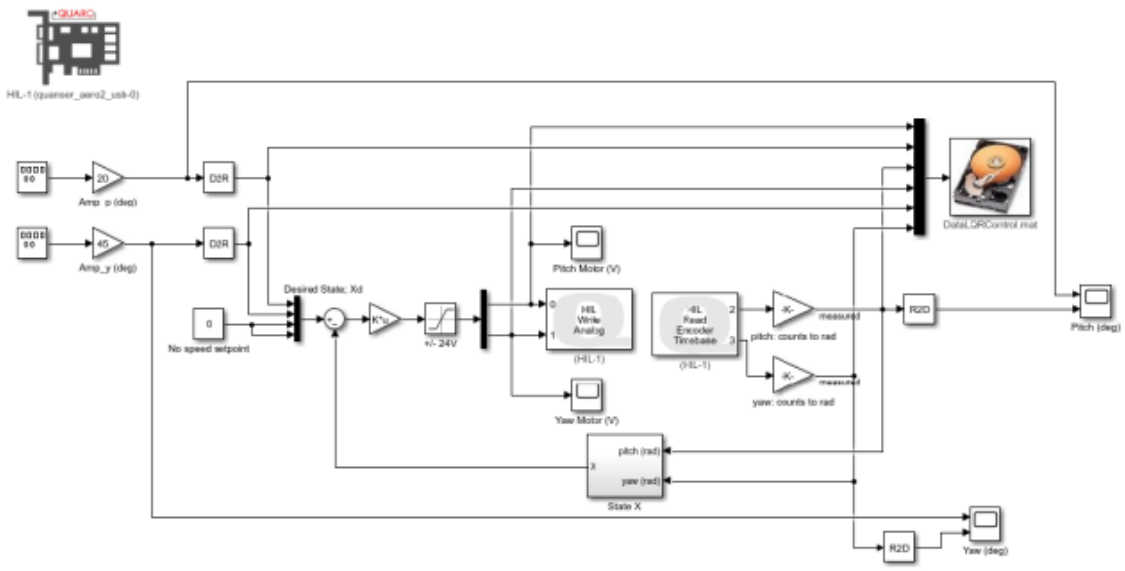

Figure III.1: Simulink model used with QUARC to run the LQR controller on the Aero2.

Figure III.2 illustrates the set up of the Quanser Aero2 system as well as the laptop where the implementation of the controllers was conducted using MATLAB/SIMULINK and the QUARC control software:

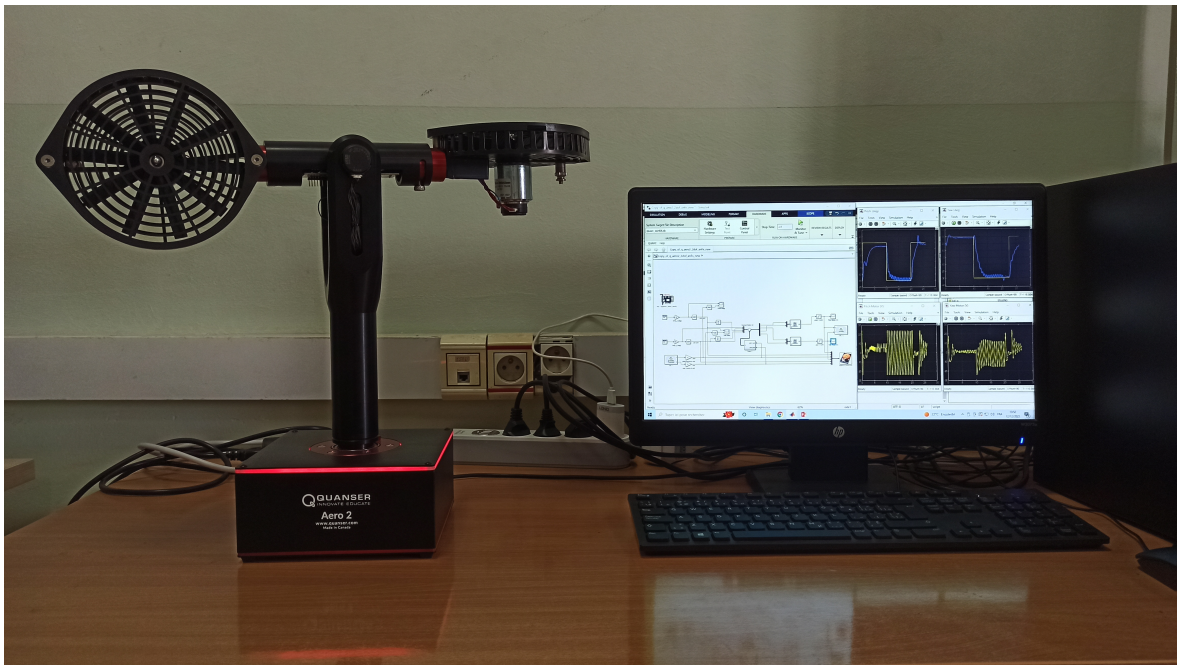

Figure III.2: The experimental setup

III.3 Experimental results

For each implementation, we followed a consistent procedure similar to the simulation. We began by initializing the Aero2 model with initial conditions set to zero. To assess the system's ability to accurately follow desired signals, we used a sinusoidal function as the input signal:

$$\begin{cases} \theta_d = 10 \cdot \sin(2\pi \cdot 0.05 \cdot t) \\ \phi_d = 20 \cdot \sin(2\pi \cdot 0.04 \cdot t) \end{cases} \tag{III.1}$$

Additionally, we employed a square function to evaluate the system's tracking performance. The pitch signal had an amplitude of 10 degrees and a frequency of 0.05 Hertz, while the yaw signal had an amplitude of 20 degrees and a frequency of 0.04 Hertz.

III.3.1 PD controller

The pitch and yaw PD control of the Aero 2 2 DOF helicopter can be implemented using the following schematic diagram :

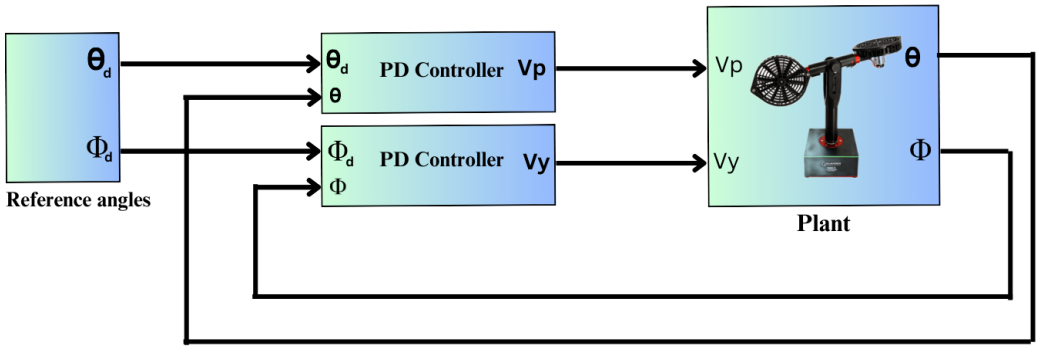

Figure III.3: PD controller implementation schematic

The controller gains used in the implementation are listed in Table III.1:

Pitch	$k_{p_p} = 116.2420$	$k_{d_p} = 99.6990$
Yaw	$k_{p_y} = 35.8626$	$k_{d_y} = 38.0289$

Table III.1: The gains for the PD controller implementation

III.3.1.1 Sinusoidal waveform tracking

The graph in Figure III.4 illustrates the desired angles and the corresponding actual angles achieved during the implementation of the PD controller , along with the output voltages applied to the front/pitch motor and tail/yaw motor.

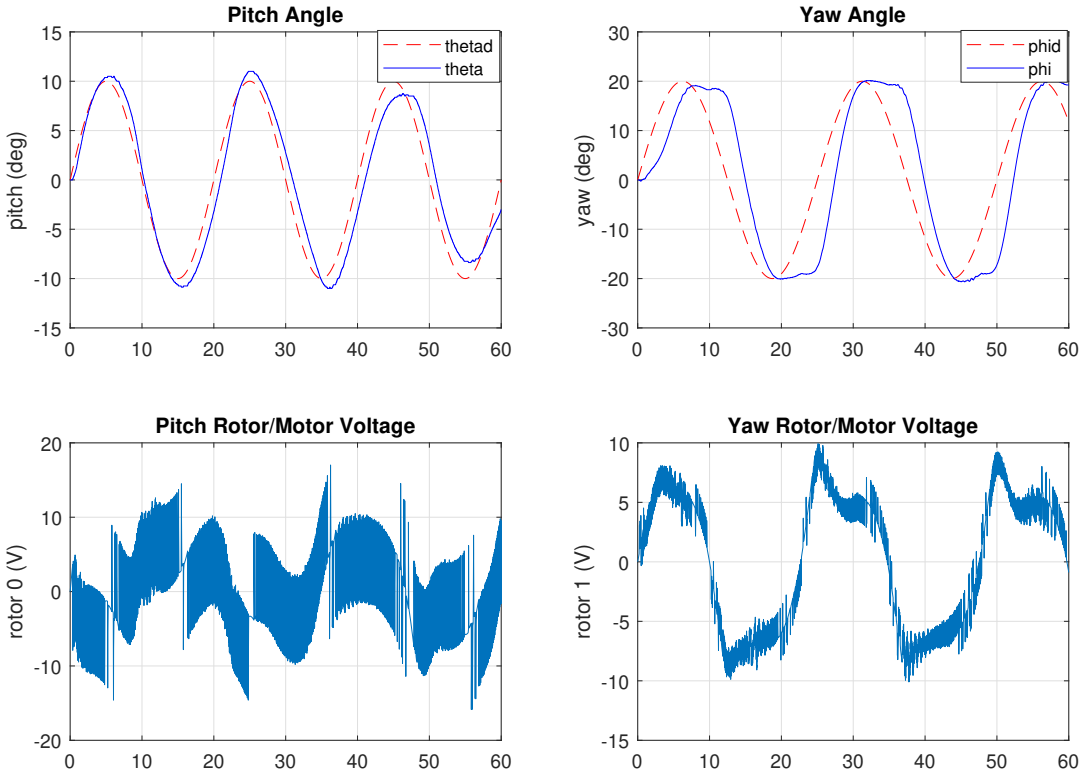

Figure III.4: Hardware response using PD controller for sinusoidal tracking

The results clearly show the ability of the PD controller to accurately track the system angles in the real-time implementation. However, it is observed that the tracking of the desired angles is not as precise as in the simulation. Additionally, there is noticeable chattering in the motor voltages, along with instances of saturation. These differences can be attributed to the impact of real-world conditions on the system.

III.3.1.2 Square wave tracking

The Figure III.5 demonstrates the performance of the PD controller in tracking the desired pitch and yaw angles of the square wave input in the real time implementation. The controller demonstrates a high level of accuracy in tracking the desired angles, with minimal deviations observed. This indicates the effective regulation of the system towards the desired operating point by the PD controller. However, it is noticed that the tracking of the desired angles is slightly less precise compared to the simulation. Furthermore, there are noticeable fluctuations in the motor voltages,as well as instances of saturation. These variations can be attributed to the influence of real-world conditions on the system.

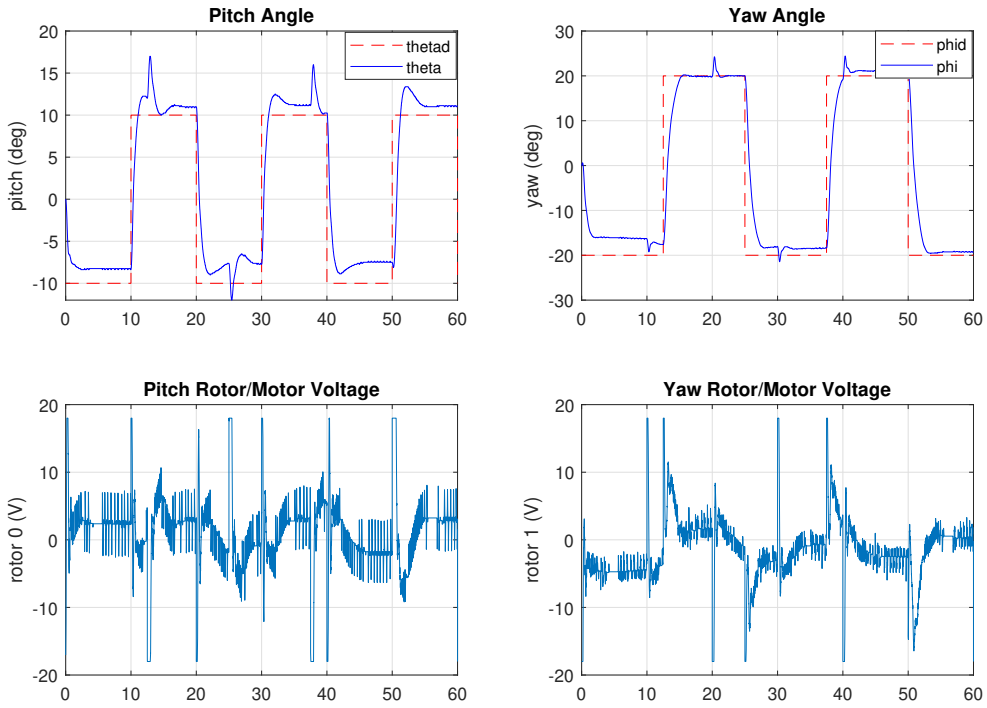

Figure III.5: Hardware response using PD controller for square tracking

III.3.2 LQR controller

The pitch and yaw LQR control of the Aero 2 - 2-DOF helicopter can be implemented using the following schematic diagram :

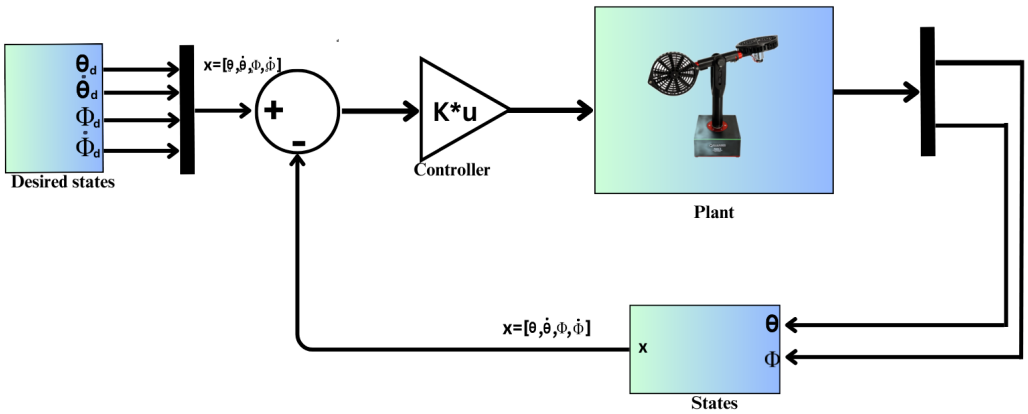

Figure III.6: LQR controller implementation schematic

Implementing the following gain matrix in the feed-back gain $u = -Kx$ illustrated in the schematic diagram of Figure III.6 :

$$K = \begin{bmatrix} 99.5844 & -37.6373 & 80.6953 & -24.3159 \\ 47.5974 & 77.9964 & 40.6478 & 52.9117 \end{bmatrix} \tag{III.2}$$

III.3.2.1 Sinusoidal waveform tracking

Figure III.7 visually illustrates the performance of the LQR controller in tracking the desired pitch and yaw angles during the implementation we cannote that the LQR outperformes the PD controller in regulating the angles.Figure III.7 also presents the output voltages corresponding to the control inputs responsible for driving the Quanser Aero2 motors. Notably, the control effort remained within the system's limits of ± 24 V. However, it is observed that the tracking of the desired angles is slightly less accurate compared to the simulation. Additionally, there are noticeable fluctuations in the motor voltages, accompanied by instances of saturation. These variations can be attributed to the impact of real-world conditions on the system.

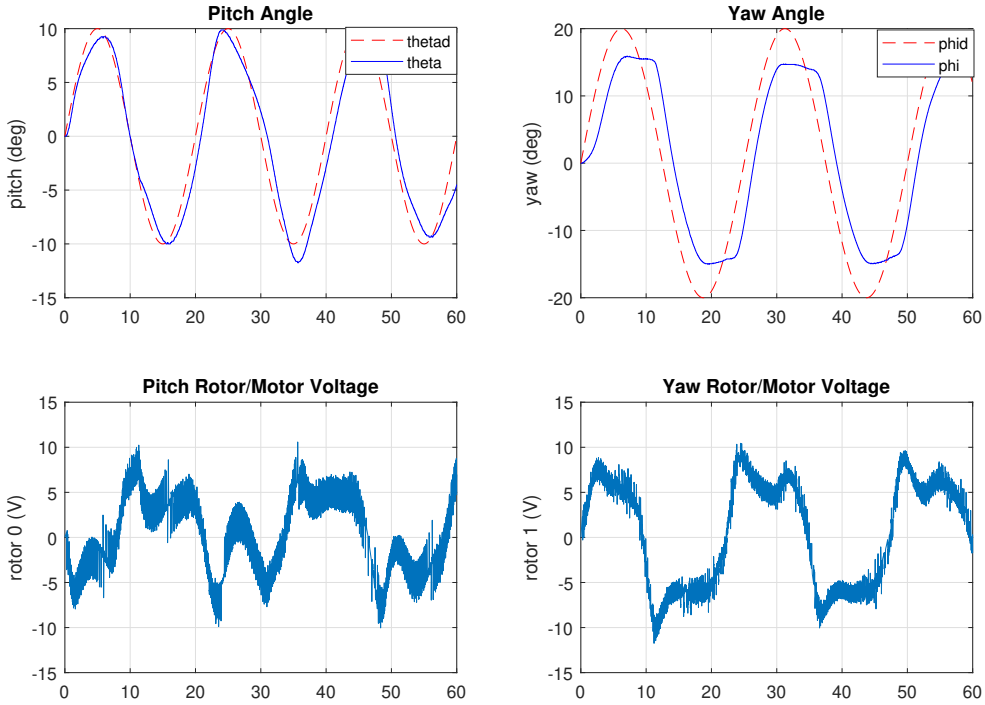

Figure III.7: Hardware response using LQR controller for sinusoidal tracking

III.3.2.2 Square wave tracking

Figure III.8 demonstrates the performance of the LQR controller in tracking the desired pitch and yaw angles subject to a square wave as desired signal . as well as the corresponding voltages applied to the motors. In contrast to the PD controller implementation, the LQR controller demonstrates enhanced performance in accurately tracking the desired angle with minimal deviations. Moreover, it exhibits smoother control actions. However, there is a slight decrease in the accuracy of tracking the desired angles compared to the simulation. Furthermore, noticeable fluctuations in the motor voltages, along with instances of saturation, are observed. These variations are mainly due to the influence of real-world conditions on the system.

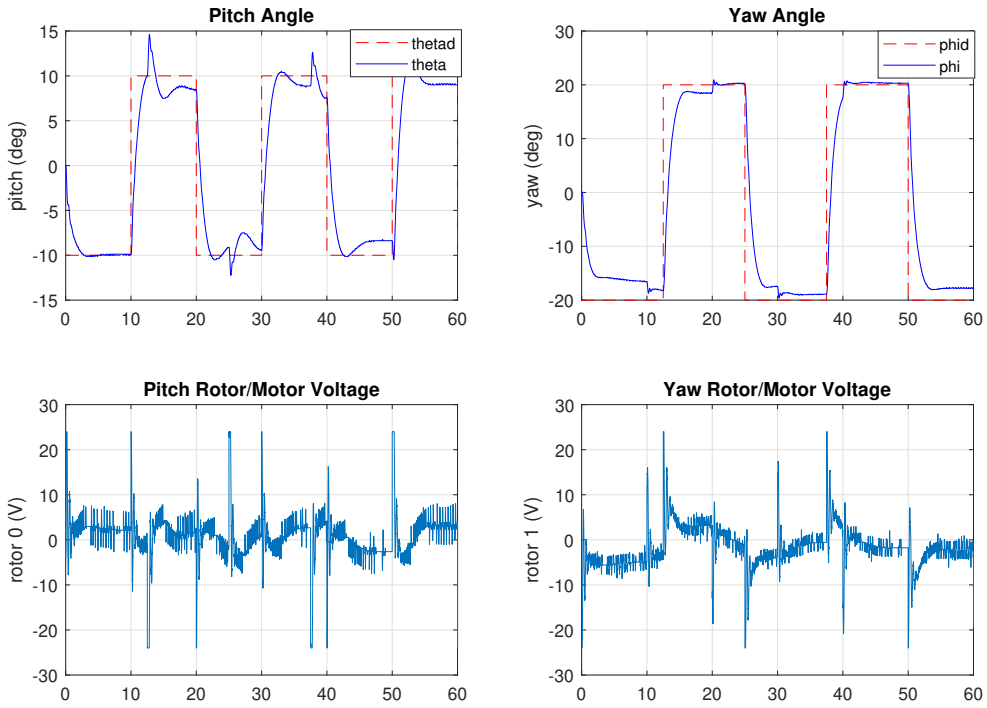

Figure III.8: Hardware response using LQR controller for square tracking

III.3.3 SM controller

The pitch and yaw SM control of the Aero 2 - 2 DOF helicopter can be implemented using the following schematic diagram :

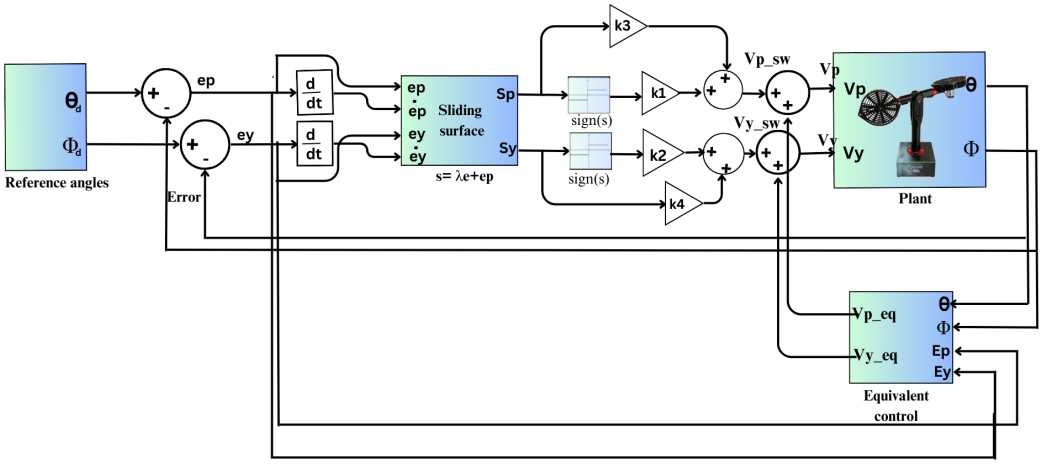

Figure III.9: SM controller implementation schematic

III.3.3.1 Sinusoidal waveform tracking

The controller gains used in the implementation are listed in Table III.2 , these parameters are different than that of the simulation, as we had to tune them again during the

real-time implementation to achieve better results and that is mainly due to the real world conditions:

Pitch	c_p=4	k_1=9	k_2=5
Yaw	c_y=2.8	k_3=8	k_4=7

Table III.2: The controller gains for the sinusoidal waveform implementation using SMC

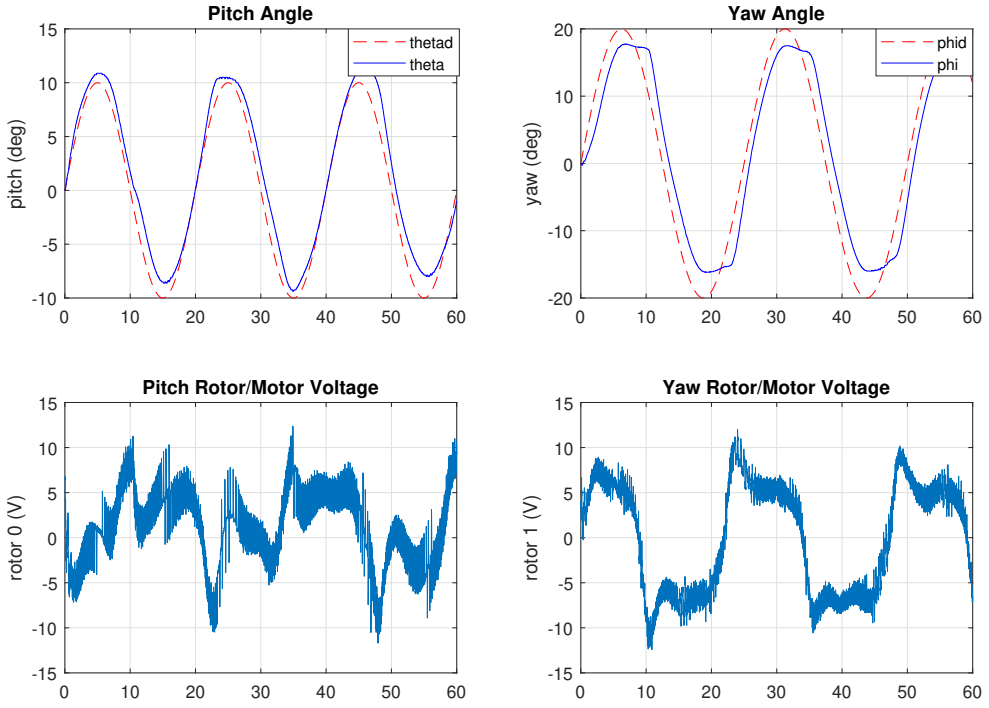

Figure III.10: Hardware response using SM controller for sinusoidal tracking

The Figure III.10 shows output angles of the Quanser Aero2 system under SMC controller with the measured voltage at the pitch and yaw motors respectively. We have effectively mitigate the chattering through the application of the hyperbolic tangent function in the controller instead of the original sign function II.49. The controller successfully tracks the desired angles. Figure III.10 also illustrate the convergence of the actual angles towards the desired angles, indicating the capability of the SMC controller to achieve accurate and stable control performance.

III.3.3.2 Square wave tracking

The values used for the controller in the real-time implementation are listed in Table III.3. It is worth mentioning that these values are different from the ones used in the

simulation. During the real-time implementation, we had to adjust and fine-tune the controller parameters again to achieve better results.

Pitch	c_p=2.5	k_1=8	k_2=1
Yaw	c_y=2.8	k_3=7	k_4=5

Table III.3: The controller gains for the square wave implementation using SMC

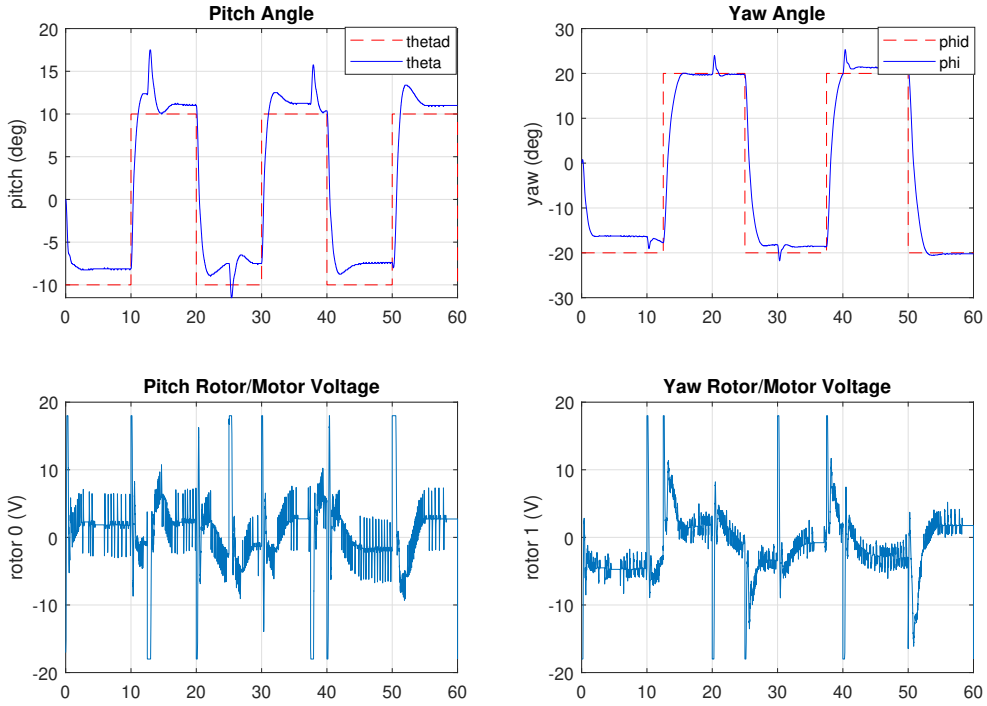

Figure III.11: Hardware response using SM controller for square tracking

Figure III.11 shows the output angles of the Quanser Aero2 system during the real-time implementation of the SM controller, where the measured voltage at the pitch and yaw motors as well as measured angles responding to a square wave signal. The use of the hyperbolic tangent function II.49 effectively mitigates chattering, resulting in improved performance compared to the linear controllers. Despite not achieving the same level of performance as the simulation, the SM controller demonstrates better tracking of the desired angles and reduced chattering in the motor voltages. These advancements signify the effectiveness of the SM .

III.3.4 ST controller

The pitch and yaw super twisting control of the Aero 2 2-DOF helicopter can be simulated using the following schematic diagram :

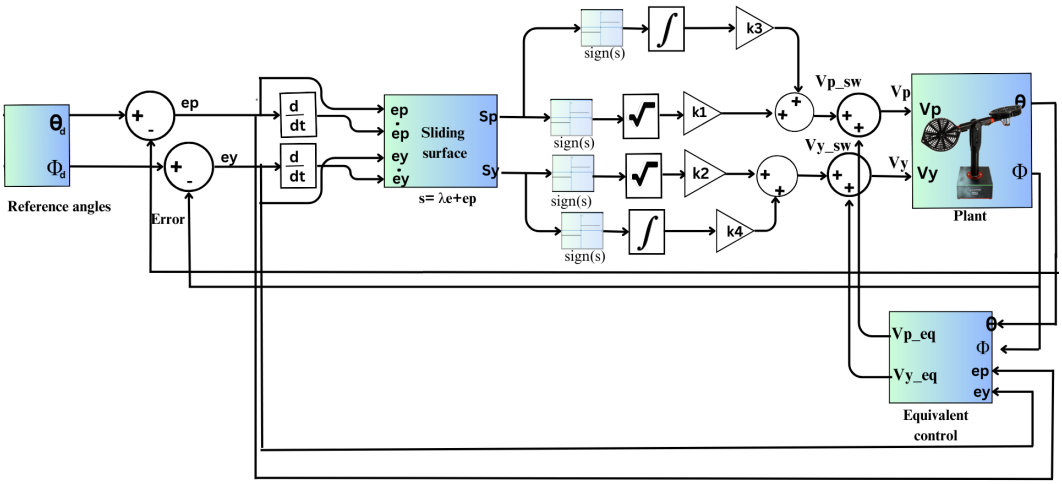

Figure III.12: Super-twisting controller implementation schematic

III.3.4.1 Sinusoidal waveform tracking

The controller gains used in the implementation can be found in Table III.4. This adjustment was necessary because we had to tune again the parameters during the real-time implementation to obtain improved results. The need for the tuning was because of the influence of real-world conditions on the system's behavior.

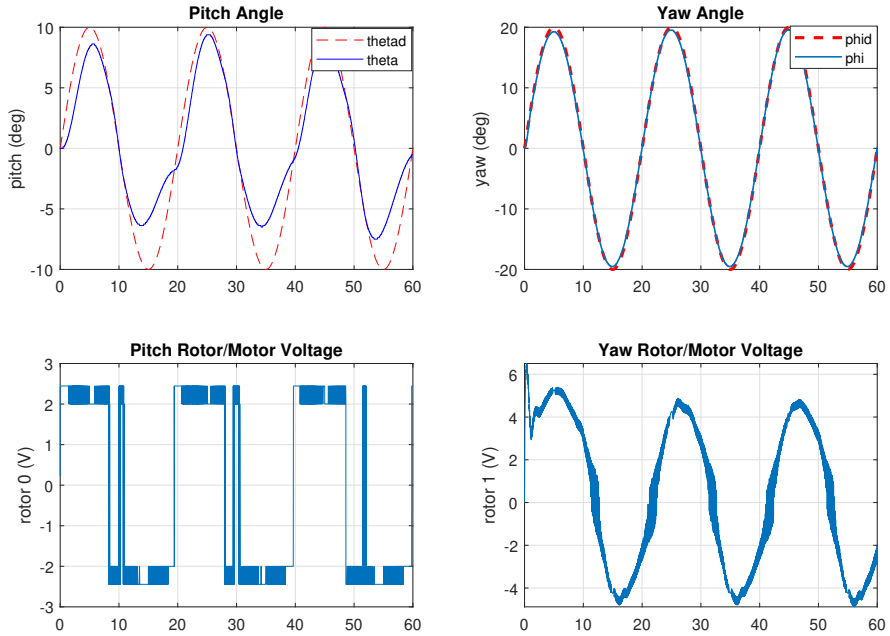

Figure III.13: Hardware response using ST controller for sinusoidal tracking

Figure III.13 displays the output pitch and yaw angles of the Quanser Aero2 system during the real-time implementation of the ST controller, with the measured voltage at the pitch and yaw motors respectively. It is observed that the performance of the controller is not as good as the simulation results, primarily due to the challenging

Pitch	c_p=50000	k_1=70	k_2=200
Yaw	c_y=89999000	k_3=70000	k_4=80000

Table III.4: The controller gains for the sinusoidal waveform implementation using STC

task of parameter tuning resulting from the strong coupling between the pitch and yaw axes as well as real world conditions . Notably, the obtained results show that the pitch angle tracking is not as successful as that of the yaw angle, primarily due to the influence of the gravitational force acting along the same axis.

III.3.4.2 Square wave tracking

The controller gains utilized in the real-time implementation are presented in Table III.5. It is important to note that these parameters differ from those employed in the simulation. During the real-time implementation, the gains had to be tuned again to optimize performance under the influence of real-world conditions. This adjustment was necessary to attain improved results and ensure effective control in practical scenarios.

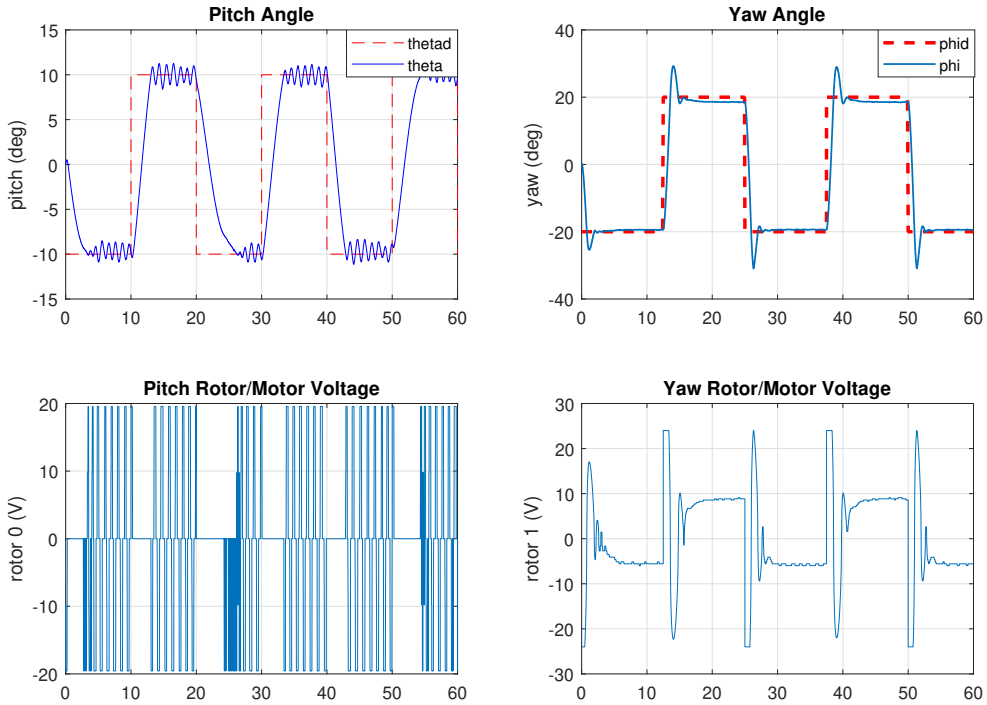

Figure III.14: Hardware response using ST controller for square tracking

Figure III.14 displays the output pitch and yaw angles of the Quanser Aero2 system during the real-time implementation of the ST controller, accompanied by the measured voltage at the pitch and yaw motors. Nonetheless, the implementation of the Super-twisting controller on the strongly coupled axes of the Quanser Aero2 model poses a

Pitch	c_p=9000	k_1=300	k_2=150
Yaw	$c_y = 10^8$	$k_3 = 8x10^5$	$k_4 = 10$

Table III.5: The controller gains for the square wave implementation using STC

challenge. The interdependence between the pitch and yaw axes adds complexity to the tuning process, demanding carefull adjustment of the controller gains to achieve stable and satisfactory performance.

III.4 Comparative Analysis of the implemented Control Strategies

In this section a comparison between the four controllers is held first by inspection of the output graphs illustrated in Figure III.15note that the PD controller demonstrates satisfactory performance in regulating the output angles, although it exhibits some steady-state error. On the other hand, the LQR controller exhibits superior performance with reduced steady-state error, thanks to its optimal control design . The SM and ST controllers exhibit good performance in achieving accurate tracking of the desired angles. they demonstrates robust performance but can be sensitive to high-frequency noise.

However, a slight problem was faced with super twisting controller in the parameter tuning because of its consideration and the coupling dynamics which is why we can notice that the performance of the yaw signal is much better than that of the pitch mainly due to the gravitational force acting on the same axes .

For a more accurate comparison of these results, we can use the performance metrics that are demonstrated in Tables III.6 and III.7 :

Response Results	PD controller	LQR controller	SM controller	ST controller
Square wave				
Overshoot ($PO\%$)	8.97	5.779	**0.505**	10.419
Peak time t_p	3	**2**	3	**2**
Rise time t_r	**1.19**	1.302	1.302	1.85
Sinusoidal waveform				
Root mean square error	7.275	**7.056**	7.071	7.15

Table III.6: Hardware response results for the pitch signal

Among the four controllers evaluated in the implementation, namely the PD (Proportional-Derivative), LQR (Linear Quadratic Regulator), SM (Sliding Mode),

Response Results	PD controller	LQR controller	SM controller	ST controller
Square wave				
Overshoot ($PO\%$)	4.316	5.779	**3.569**	7.43
Peak time t_p	2	2	2	2
Rise time t_r	4.837	1.302	1.584	**0.73**
Sinusoidal waveform				
Root mean square error	14.549	11.93	**7.15**	13.81

Table III.7: Hardware response results for the yaw signal

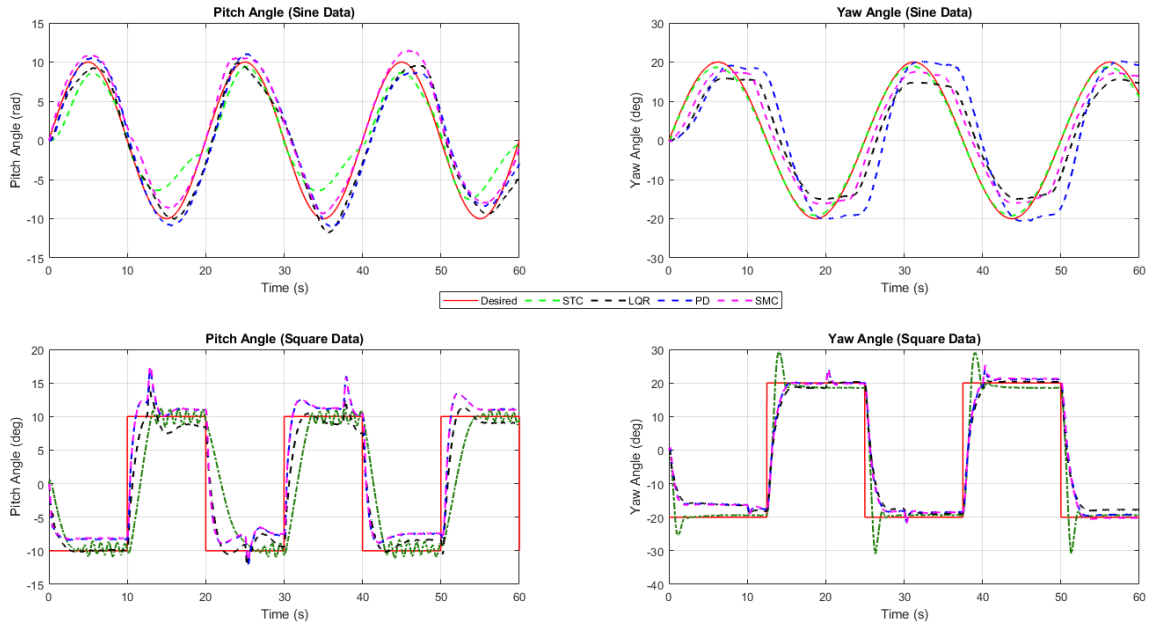

Figure III.15: Comparison of the implementation results

and ST (Super Twisting) controllers, the overshoot and rise time performances vary. In terms of overshoot for the square wave tracking , the PD controller and the super twisting controllers exhibit the highest overshoot with values of$PO = 8.97\%$ and $PO = 10.42\%$. The LQR controller performs slightly better with reduced overshoot. The SM controller shows a significant reduction in overshoot, achieving values of 0.505% and 3.569% for the pitch and yaw angles respectively ofcourse the values obtained in the implementation were not as good as the ones in the simulation and that is mainly due to real world conditions.

Moving on to rise time for the square wave tracking, the PD controller has the longest rise time with values of $t_r = 4.837s$ for the yaw signal. The SM controller performs slightly better with values of $t_r = 1.584s$ for both the pitch and yaw signals. However, The LQR controller demonstrates a significant improvement, achieving rise

times of $t_r = 1.302s$ for both the pitch and yaw signals. The ST controller performs well in terms of rise time achieving the lowest result for the yaw angle being $t_r = 0.731s$.

considering the root mean square error for the sinusoidal waveform tracking the LQR exhibits the best performance with values of 7.056 and 11.93 for the pitch and yaw angles respectively the SMC controller exhibits good performance in terms of root mean square error achieving values of 7.071 and 7.15 for the pitch and yaw angles respectively.

Based on the analysis of the performance metrics presented in Tables III.6 and III.7, it can be concluded that the LQR and SMC controllers demonstrate superior performance in the real-time implementation among the four controllers.

Considering the characteristics of each tested controller, we can conclude that the PD controller is suitable for basic control tasks, while the LQR controller offers optimal performance when an accurate model is available. The SM and ST controllers provide robustness against uncertainties and disturbances but require careful tuning, especially for highly coupled systems like the Quanser Aero2.

III.5 Conclusion

This chapter covered the real-time implementation of the developed linear and nonlinear controllers on the Quanser Aero2 platform following the same procedure as the simulation by introducing the sinusoidal and square waveforms as desired inputs .However, we encountered a challenge during parameter tuning, where we had to adjust the implementation parameters once again to achieve improved results in real-time implementation. This was mainly due to the influence of real-world conditions.A comparative study of the obtained results was conducted to evaluate the effectiveness and performance of the implemented controllers.

Chapter IV

Implementation and results

IV.1 Introduction

In this chapter the focus is on the practical realization of the control strategies (PD, LQR, and SMC) for the 2-DOF Helicopter Quanser Aero2 system. This chapter provides a detailed account of the hardware setup, software development, and integration of the control algorithms with the physical system. The objective is to demonstrate the feasibility and effectiveness of each control strategy in a real-world scenario. Performance evaluation and comparison of the implemented controllers are conducted using various metrics to assess their stability, tracking accuracy, and robustness.

General conclusion and perspectives

This work contributes to the field by presenting various models of the Quanser Aero2 system and integrating them to design multiple controllers. The objective of is to develop models, conduct simulations, and implement real-time controllers for the Quanser Aero2 2-DOF helicopter. The performance of these controllers is evaluated and compared.

The nonlinear model of the Quanser Aero2 system, along with its linear models are presented both in transfer function and state space forms. These models are later used in the design of two classical control techniques : Proportional Derivative (PD), Linear Quadratic Regulator (LQR), as well as two nonlinear control techniques : Sliding Mode Controller (SMC), and Super Twisting Controller (STC)

The PD, LQR, SMC, and STC controllers are designed and simulated using MATLAB/SIMULINK. The performance of each controller is evaluated and compared through simulation results. Furthermore, all four controllers are tested in realt time implementation on the Quanser Aero2 platform by using QUARC software . The evaluation and comparison of these controllers are conducted based on the results of pitch and yaw angles with their corresponding voltages, as well as performance metrics such as percentage overshoot and rise time...etc

The results demonstrate that the mentioned controllers efficiently and effectively track the desired angles, with slight variations in performance. Notably, the sliding mode controller and the super twisting controllers, exhibit superior performance compared to classical control techniques .However, we encountered a challenge during parameter tuning, where we had to adjust the implementation parameters once again to achieve improved results in real-time implementation. This was mainly due to the influence of real-world conditions.

For future investigations, it is recommended to address the challenges associated with tuning of the parameters of the nonlinear controllers.

- Exploring techniques such as fuzzy logic, Neural Networks, or any metaheuristic algorithm to adaptively adjust controller parameters can be of great interest and can potentially enhance the performance and overcome the highly nonlinear dynamics and cross-coupling exhibited by the Quanser Aero2 2-DOF helicopter.

- Conducting a study on the robustness of the controllers under uncertainties and external disturbances. One approach could involve incorporating a fan in the implementation to simulate wind and evaluate the controllers' performance in such conditions.
- Alternative techniques, such as reinforcement learning and model predictive control, can also be employed to address the coupled nonlinear model of the Quanser Aero2 system without relying on explicit modeling.

Bibliography

[1] W. J. Boyne. (2023) helicopter. Encyclopedia Britannica. [Online]. Available: https://www.britannica.com/technology/helicopter

[2] "16 types of helicopters – civilian helicopters and military helicopters [with pictures & names]," *Engineering Learn*, 2023. [Online]. Available: https://engineeringlearn.com/16-types-of-helicopters-civilian-helicopters-and-military-helicopters-with-pictures-names/

[3] Sikorsky Aircraft Corporation, "Sikorsky x2 technology demonstrator," 2008. [Online]. Available: https://www.sikorskyarchives.com/X2.php

[4] NASA, "Ingenuity mars helicopter," 2021. [Online]. Available: https://www.nasa.gov/mission_pages/mars-helicopter/

[5] J. Smith, "Operating principles of helicopters," *Aerospace Engineering Review*, vol. 36, no. 3, pp. 245–259, 2022.

[6] J. G. Leishman, *Introduction to Aerospace Flight Vehicles*. Embry-Riddle Aeronautical University, January 2023.

[7] Quanser Inc., "Quanser aero 2 data sheet," https://www.quanser.com/products/quanser-aero-2/, 2022.

[8] ——, "Quanser aero 2 user manuel," 2022.

[9] Q. Inc., *Quanser AERO2 - 2DOF Lab Guide*, 20XX. [Online]. Available: https://www.quanser.com/wp-content/uploads/20XX/XX/Quanser-AERO2-2DOF-Lab-Guide.pdf

[10] R. Patel, D. Deb, H. Modi, and S. Shah, "Adaptive backstepping control scheme with integral action for quanser 2-dof helicopter," *2017 International Conference on Advances in Computing, Communications and Informatics (ICACCI)*, 2017.

[11] M. W. Spong, S. Hutchinson, and M. Vidyasagar, *Robot Modelling and Control*. John Wiley Sons, 2006.

[12] C. Lanczos, *The Variational Principles of Mechanics*. Courier Corporation, 1970.

[13] R. C. Dorf and R. H. Bishop, *Modern Control Systems*. Pearson, 2011.

[14] X. Ying, Q. Zhi-Chang, and S. Jian-Qiao, "Input-output tracking control of a 2-dof laboratory helicopter with improved algebraic differential estimation," *Mechanical Systems and Signal Processing*, vol. 116, pp. 843–857, February 2019.

[15] S. Sadala and B. Patre, "A new continuous sliding mode control approach with actuator saturation for control of 2-dof helicopter system," *ISA Transactions*, vol. 74, pp. 165–174, March 2018.

[16] Z. Jiang and K. Karim, "Application of adaptive sliding mode control for nonlinear systems with unknown polynomial bounded uncertainties," *Transactions of the Institute of Measurement and Control*, vol. 40, no. 13, pp. 3721–3735, 2018.

[17] C. C. Ko, B. M. Chen, J. Chen, J. Zhang, and K. C. Tan, "A web-based laboratory on control of a two-degrees-of-freedom helicopter," *Department of Electrical and Computer Engineering, The National University of Singapore*, 2023.

[18] E. Vinodh Kumar, G. S. Raaja, and J. Jerome, "Adaptive pso for optimal lqr tracking control of 2 dof laboratory helicopter," *Applied Soft Computing*, vol. 41, pp. 77–90, 2016. [Online]. Available: https://www.sciencedirect.com/science/article/pii/S1568494615008029

[19] R. G. Subramanian and V. K. Elumalai, "Robust mrac augmented baseline lqr for tracking control of 2 dof helicopter," *Robotics and Autonomous Systems*, vol. 86, pp. 70–77, 2016. [Online]. Available: https://www.sciencedirect.com/science/article/pii/S0921889015302864

[20] P. Lambert and M. Reyhanoglu, "Observer-based sliding mode control of a 2-dof helicopter system," *Mechanical Engineering Department, Eindhoven University of Technology*, 2016.

[21] S. Kumar and L. Dewan, "A comparative analysis of lqr and smc for quanser aero control and measurement applications for smart grid," in *Volume 822*, 2022.

[22] Q. Ahmed, A. Bhatti, S. Iqbal, and I. Kazmi, *2-sliding mode based robust control for 2-DOF helicopter*, 2010/07/28.

[23] M. Reyhanoglu, M. Jafari, and M. Rehan, "Simple learning-based robust trajectory tracking control of a 2-dof helicopter system," *Sensors*, vol. 22, no. 5, p. 2374, 2022.

[24] K. J. Aström and T. Hägglund, "Pid controllers: theory, design, and tuning," *Instrument Society of America*, vol. 5, no. 1, pp. 1–32, 2001.

[25] K. J. Å ström and R. M. Murray, "Feedback systems: an introduction for scientists and engineers," 2008.

[26] A. Levant, "Robust exact differentiation via sliding mode technique," *Automatica*, vol. 34, no. 3, pp. 379–384, 1998.

[27] J. Slotine and W. Li, *Applied Nonlinear Control*, 1st ed. Englewood Cliffs, NJ: Prentice Hall, 1991.

[28] A. Kowalewski *et al.*, "Robust sliding mode control for a quadrotor uav," in *Proceedings of the 19th International Conference on Methods and Models in Automation and Robotics*, 2014, pp. 710–715.

[29] B. Brahim *et al.*, "Sliding mode control for nonlinear systems: A design perspective," *International Journal of Control, Automation and Systems*, vol. 7, no. 3, pp. 419–432, 2009.

[30] R. Bento *et al.*, "Sliding mode control: From theory to applications," *International Journal of Control, Automation and Systems*, vol. 14, no. 1, pp. 1–10, 2016.

[31] M. Furat and I. Eker, "Experimental evaluation of sliding mode control techniques," *International Journal of Electrical, Computer, Energetic, Electronic and Communication Engineering*, vol. 6, no. 1, pp. 99–104, 2012.

[32] H. K. Khalil, *Nonlinear Systems*. Prentice Hall, 2002.

[33] A. Levant, "Chattering analysis," *IEEE Transactions on Automatic Control*, vol. 55, no. 6, pp. 1380–1389, 2010.

[34] A. Benchaib and L. Fridman, "Design of variable structure systems with sliding mode by second-order sliding mode," *International Journal of Control*, vol. 72, no. 7-8, pp. 612–620, 1999.

[35] V. I. Utkin and B. G. Levant, "Sliding order and sliding accuracy in sliding mode control," *International Journal of Control*, vol. 58, no. 6, pp. 1247–1263, 1993.

[36] Y. Zhou, C. Chen, and J. Chen, "Super-twisting algorithm for second-order sliding mode control," *Journal of the Franklin Institute*, vol. 353, no. 2, pp. 475–492, 2016, discusses the working principle of the Super Twisting Controller and its sliding mode approach with a switching function.

[37] A. J. Humaidi and A. F. Hasan, "Particle swarm optimization–based adaptive super-twisting sliding mode control design for 2-degree-of-freedom helicopter," *Measurement and Control*, vol. 52, no. 9-10, pp. 1403–1419, 2019, date received: 6 March 2019; accepted: 2 June 2019.

[38] "Quanser website," https://www.quanser.com.

Appendix A

Appendix A

A.1 Component specifications of the Quanser Aero2

Table A.1 lists and characterizes the parameters of the 2-DOF helicopter system.

Table A.1: Quanser Aero 2 System Parameters [8]

Symbol	Description	Value	Units
	DC Motor		
V_{nom}	Nominal input voltage	18.0	Volts
τ_{nom}	Nominal torque	22.0	mN · m
$\dot{\omega}_{\text{nom}}$	Nominal angular velocity	3050	RPM
I_{nom}	Nominal current	0.540	Amps
R_m	Terminal resistance	8.4	Ω
k_t	Torque constant	0.042	N · m
$\frac{A}{k_m}$	Motor back-EMF constant	0.042	V/(rad/s)
J_m	Rotor inertia	4.0×10^{-6}	kg · m^2
L_m	Rotor inductance	1.16	mH
	Aero Body		
M_b	Mass of body	1.07	kg
D_m	Displacement of Center of Mass (z-axis)	0.0024	mm
D_t	Thrust displacement	0.168	m
	Amplifier		
Amplifier type	PWM	-	-
Peak current	2	Amps	-
Continuous current	0.5	Amps	-
Output voltage range (recommended)	±18	Volts	-
Output voltage range (maximum)	±24	Volts	-

A.2 Parameter estimation

In order to characterise the parameters that are not accurately given in the user manual we have estimated them. The equation of motion for a second-order system under free-oscillation conditions can be expressed as [9] :

$$J\ddot{\alpha} + D\dot{\alpha} + K\alpha = 0 \tag{A.1}$$

If the initial conditions are given by $\alpha(0^-) = \alpha_0$ and $\dot{\alpha}(0^-) = 0$,then Equation(A.1) can be transformed using Laplace transform as follows:

$$\alpha(s) = \frac{\frac{\alpha_0}{J}}{s^2 + \frac{D}{Js} + \frac{K}{J}} \tag{A.2}$$

The prototype second-order equation is defined as :

$$s^2 + 2\zeta\omega_n s + \omega_n^2 \tag{A.3}$$

The natural frequency of a system can be determined by using the following equation, which relates the period of oscillations in the system response:

$$T_{osc} = \frac{t_n - t_1}{n - 1} \tag{A.4}$$

By considering the time of the first peak as ($t_1 = 71.25$ s), and the time of the nth oscillation as ($t_n = 142.6$ s), where n represents the number of oscillations ($n = 8$), the natural frequency of the system can be determined. The damped natural frequency, expressed in radians per second, can be calculated as follows[9]:

$$\omega_d = \frac{2\pi}{T_{osc}} \tag{A.5}$$

and the undamped natural frequency is:

$$\omega_n = \frac{\omega_d}{\sqrt{1 - \zeta^2}} \tag{A.6}$$

To determine the damping ratio of a second-order system, its response can be analyzed. In the case of a standard underdamped second-order system, the subsidence ratio, also known as the decrement ratio, is a useful parameter. This ratio is defined as follows:

$$\delta = \frac{1}{n} \ln\left(\frac{O_1}{O_n}\right) \tag{A.7}$$

where ($O_1 = 0.218°$) is the peak of the first oscillation and ($O_n = 0.0131°$) is the peak of the n th oscillation. Note that:$O_1 > O_n$, as this is a decaying response. The damping ratio can then be found by:

$$\zeta = \frac{1}{\sqrt{1 + \frac{2\pi}{\delta^2}}} \tag{A.8}$$

A.2.1 Estimating the viscous damping coefficients :

The equations of motion for the actuated system with only 1 DOF are obtained[9].

$$J_p\ddot{\theta}(t) + D_p\dot{\theta}(t) + K_{sp}\theta(t) = 0 \tag{A.9}$$

Taking its Laplace transform gives :

$$J_p(\Theta(s)s^2 - \theta(0^-)s - \dot{\theta}(0^-)) + D_p(\Theta(s) - \theta(0^-)) + K_{sp}\Theta_p(s) = 0 \tag{A.10}$$

Assuming the initial velocity is zero, $\dot{\theta}(0^-) = 0$, and solving for position we get:

$$\Theta(s) = \frac{J_p}{J_p s^2 + D_p s + K_{sp}}, \quad \theta(0^-) = \frac{J_p/D_p}{s^2 + D_p/J_p + K_{sp}/J_p} \tag{A.11}$$

The pitch free-oscillation transfer function is in agreement with the standard second-order transfer function given in eq (A.2) Using the measured natural frequency and damping ratio of the response, the friction or stiffness of the system can be determined.

$$K_{sp} = J_p\omega_n^2, \qquad K_{sp} = 0.00884 \text{ N-m/rad} \tag{A.12}$$

and the viscous damping is:

$$D_p = 2\zeta\omega_n J_p, \qquad D_p = 0.0199 \text{ N-m/(rad/s)} \tag{A.13}$$

For yaw axis The equations of motion for yaw-only motion in a single degree of freedom (1 DOF) are given by:

$$J_y\ddot{\psi} + D_y\dot{\psi} = K_{yy}D_tV_y \tag{A.14}$$

In terms of angular rate, the equation becomes:

$$Jy\omega_y(t) + Dy\dot{\omega}_y(t) = 0 \tag{A.15}$$

where $\omega_y(t) = \dot{\psi}(t)$. Taking its Laplace transform:

$$J_p(\Omega_y(s)s - \omega_y(0^-)) + D_p\Omega_y(s) = 0 \tag{A.16}$$

and solving for the speed we get :

$$\Omega_y(s) = \frac{J_y}{J_y s + D_y}\omega_y(0^-) \ \omega_y(0^-) = \frac{J_y/D_y}{J_y/D_y s + 1} \tag{A.17}$$

The transfer function for free-oscillatory yaw motion matches the prototype first-order transfer function. By determining the time constant of the response, the damping can be obtained using [9]:

$$D_y = J_y/\tau. \qquad D_y = 0.00192N - m/(rad/s) \tag{A.18}$$

A.2.2 Estimating the thrust parameters :

The equations of motion for the actuated system with only 1 DOF are obtained.

$$J_p\ddot{\theta} + D_p\dot{\theta} + K_{sp}\theta = K_{pp}V_p \tag{A.19}$$

The pitch equation is obtained by considering angular rate and incorporating the stiffness estimate in the analysis

$$J_p\dot{\omega}_p + D_p\omega_p = K_{pp}V_p \tag{A.20}$$

Where $\omega_p = \dot{\theta}$ is the angular rate of the pitch axis. Solving for the thrust gain we get:

$$K_{pp} = \frac{J_p\dot{\omega}_p + D_p\omega_p}{V_p} = 0.00321 \text{ N/V} \tag{A.21}$$

The following representation of the system is obtained whe[9]:

$$J_y\ddot{\psi} + D_y\dot{\psi} = K_{yy}V_y \tag{A.22}$$

Or,

$$J_y\dot{\omega}y + D_y\omega_y = KyyV_y \tag{A.23}$$

where $\omega_y = \dot{\psi}$ is the angular rate of the yaw axis. The yaw torque thrust gain is

$$K_{yy} = J_y\dot{\omega}_y + D_y\omega_yV_y. \tag{27}$$

Therefore,

$$K_{yy} = 0.00610 \text{ N/V}. \tag{A.24}$$

The parameters Kpy and Kyp indicate the interdependence of the two axes . The equations that describe the dynamic when a voltage is applied to the tail rotor and $Vp = 0V$ is as follows [9]:

$$J_p\ddot{\theta} + D_p\dot{\theta} = K_{py}V_y \tag{A.25}$$

Putting this in terms of angular rate, $\omega_p = \dot{\theta}$, and solving for the gain we get

$$K_{py} = J_p\dot{\omega}_p + D_p\omega_pV_y \tag{A.26}$$

Therefore,

$$K_{py} = 0.00137N/V \tag{A.27}$$

Then we determine the gain parameter for cross-torque generated around the yaw axis by a pitch torque, the following equation can be used:

$$J_y\ddot{\psi} + D_y\dot{\psi} = K_{yp}V_p \tag{A.28}$$

and the gain can be found using:

$$K_{yp} = J_y\dot{\omega}_y + D_y\omega_y V_p K_{yp} = -0.00319 \text{ N/m} \tag{A.29}$$